Assessing the Interfacial Activity of Insoluble Asphaltene Layers: Interfacial Rheology versus Interfacial Tension

Alexandra Alicke,[†] Sébastien Simon,[‡] Johan Sjöblom,[‡] and Jan Vermant[*,†]

[†]*Department of Materials, ETH Zurich, Vladimir-Prelog-Weg 5, Zurich 8093, Switzerland*

[‡]*Department of Chemical Engineering, Ugelstad Laboratory, NTNU, N-7491 Trondheim, Norway*

E-mail: jan.vermant@mat.ethz.ch

Abstract

Asphaltenes have been suggested to play an important role in the remarkable stability of some water-in-crude oil emulsions, although the precise mechanisms by which they act are not yet fully understood. Being one of the more polar fractions in crude oils, asphaltenes are surface active and strongly adsorb at the oil/water interface, and as the interface becomes densely packed, solid-like mechanical properties emerge which influence many typical interfacial experiments. The present work focuses on purposefully measuring the rheology in the limit of an insoluble, spread Langmuir monolayer in the absence of adsorption/desorption phenomena. Moreover, the changes in surface tension are deconvoluted from the purely mechanical contribution to the surface stress using experiments with precise interfacial kinematics. Compression 'isotherms' are combined with the measurement of both shear and dilatational rheological properties to evaluate the relative contributions of mechanical vs. thermodynamics aspects, i.e. to evaluate the "interfacial rheological" versus the standard interfacial activity. The experimental

results suggest that asphaltene nanoaggregates are not very efficient in lowering interfacial tension, but rather impart significant mechanical stresses. Interestingly, physical ageing effects are not observed in the spread layers, contrary to results for adsorbed layers. By further studying asphaltene fractions of different polarity, we investigate whether mere packing effects or strong interactions determine the mechanical response of the dense asphaltene systems, as either soft glassy or gel-like responses have been reported. The compressional and rheological data reflect the dense packing and the behavior is captured well by the soft glassy rheology model, but a more complicated multilayer structure may develop as coverage is increased. Potential implications of the experimental observations on these model and insoluble interfaces for water-in-crude oil emulsion stability are briefly discussed.

Introduction

The stability of water-in-crude oil emulsions poses a big challenge to the oil industry. These emulsions are usually formed in oil wells as the crude oil flows together with water originated either from the subsurface formation or from enhanced oil recovery (EOR) methods. When flowing through pumps, chokes, or valves, both phases get mixed at high shear rates, leading to emulsification of the water in the oil. This causes transportation problems and cost increase because of the higher viscosity of emulsions when compared to the pure oil. In addition, separation problems arise from increased difficulty in removing water to acceptable levels, and moreover the entrapped water can lead to corrosion in separation facilities[1,2]. The presence of asphaltenes is considered a key reason for the difficulty to destabilize these emulsions and separate the water, although the precise mechanisms by which asphaltenes act are still not fully understood[3,4]. Demulsifiers are often added and whereas their environmental impact is already being decreased, a better understanding of mechanisms of stabilization could lead to a more optimized dosing.

Asphaltenes are defined as those crude oil components which are insoluble in alkanes, but

are soluble in toluene. That is, they are not defined by molecular structure or functionality, but rather by their solubility class. The consequence is that a multitude of different molecules with different functionalities can be present[5,6] and asphaltenes can differ greatly from one source to another. For this reason, characterization of asphaltenes is not straightforward and there are diverging views in literature, which make a commonly agreed upon understanding on asphaltene behavior rather difficult. Due to this variability, results are usually reported and discussed in terms of 'average properties' of asphaltenes, e.g. average molecular weight. The molecular structure of asphaltenes has long been debated, until Schuler et al.[7] visualized and confirmed a variety of molecular structures. The "island model" seems to be the dominant chemical species, i.e. a molecule composed of one main aromatic core with peripheral alkyl chains, although the size and type of polycyclic aromatic hydrocarbons (PAH) may vary. It has been recently suggested[8] though that this prevalence of the island molecule can be related to sample origin. Yet, despite the chemical diversity there seems to be a consensus that asphaltenes tend to aggregate in a similar way[9,10]. There are two main views describing this general aggregation behavior, namely the Yen-Mullins[11] model and the supramolecular assembly model[12], with the first being currently the most widely used. In this model, the picture is that at very low concentrations asphaltenes are expected to be present as isolated molecules. At intermediate concentrations, above the so-called critical nanoaggregate concentration (CNAC) of $\sim$ 100mg/L, the molecules self-assemble, most likely by stacking of the polycyclic aromatic cores to form the nanoaggregates. These nanoaggregates are believed to comprise a few molecules as the surrounding alkyl chains tends to limits its size. At higher concentrations these aggregates form clusters, which have smaller binding energies than the ones occurring within the nanoaggregates. Molecular dynamics simulations (MD) and dissipative particle dynamics (DPD) are consistent with the presence of nanoaggregates, in bulk[13–15], and at liquid-liquid interfaces[16,17].

Asphaltenes are typically one of the more polar fractions in crude oils and their chemical nature, and possibly their colloidal nature (when present as nanoaggregates), makes them

prone to strongly adsorb at the oil/water interface, due to the high capillary energy of colloidal nanoaggregates[18]. Asphaltene adsorption does however not only lead to a change in interfacial tension, but the formation of elastic skins around droplets has been reported[3,19–21]. These films macroscopically wrinkle upon compression, a clear signature of their solid-like nature. It has been proposed that this elastic film is formed by a physically cross-linked network of asphaltenes[4,22–25] and it has been suggested to suppress coalescence. However, other groups have argued that rather than attractive interactions leading to a gel, the high packing density leads to a soft-glassy type behaviour[26,27]. Pauchard et al called it an interfacial "jamming" caused by limited coalescence[28] with surface concentration being $\sim$3.5 mg/m^2. This value where interfaces become crowded and relaxations become arrested seems similar for different asphaltene systems[29]. However, currently there is no consensus on whether the interfacial layers should be viewed as mere dense 2D suspensions or whether they are interfacial gels[30,31]. In the present work we will compare the surface activity and interfacial rheology of different asphaltene fractions, as differences in polarity should lead to differences in interfacial forces and potential physical cross-linking. This should provide clarity on whether the interfacial forces and subsequent gelation, or mere crowding determine the behavior.

Different techniques have been used to investigate the interfacial rheological behavior of asphaltene interfaces as reviewed by Simon et al.[32], but it is not always clear if and when intrinsic material properties are measured. In particular for experiments with a significant dilatational or compressional deformation, the effects of compressibility and interface mechanics are often difficult to separate[33–35]. For interfaces such as dense asphaltene layers, the total interfacial stress can be written as being composed of an interfacial tension (or pressure) and an extra interfacial stress component which arises due to deformations of the interface:

$$\sigma_{\mathbf{s}} = \sigma_{\alpha\beta}(\Gamma, T)\mathbf{I} + \sigma_{\mathbf{e}} \qquad . \tag{1}$$

At a constant temperature (T), the state variable $\sigma_{\alpha\beta}$ will only on the surface concentration Γ. The extra stress σ_e can contain both isotropic and deviatoric contributions: the deviatoric stresses can be probed with shear rheology by keeping the size of interfacial area constant and then shearing it, while the isotropic stresses can be measured with dilatational rheology by inducing area changes without changing its shape. With respect to interfacial shear rheology, mostly the effects of ageing, asphaltene (bulk) concentration, solvent aromaticity, and adsorption times on the viscoelastic moduli ($G_i^{'}$ and $G_i^{''}$) have been studied[36–38]. Major findings include that the interface becomes increasingly elastic with ageing time and bulk concentration.

Dilatational rheological properties are typically investigated using the pendant drop device or Langmuir-Pockels troughs[21,24,39,40]. Most studies report an (apparent) elasticity calculated from changes in interfacial tension as a function of area changes, that is inherently based on the definition of the Gibbs elasticity K_Π:

$$K_\Pi = \frac{d\,\sigma_{\alpha\beta}}{d\,\ln\,A} \tag{2}$$

Specifically, in oscillating droplet and oscillating barrier experiments a frequency-dependent complex dilatational modulus $K^*(\omega)$ is calculated and then decomposed into its elastic (K') and viscous (K'') contributions. It is also common practice in literature to quantify dilatational behavior in terms of an apparent compressional modulus (K_{app}), which can be calculated from the slope of compression isotherms as

$$K_{app} \approx -\frac{\Pi_1 - \Pi_2}{\ln(A_1) - \ln(A_2)} \tag{3}$$

where Π is the surface pressure, defined as $\Pi(\Gamma) = \sigma_0 - \sigma_{\alpha\beta}(\Gamma)$, i.e. the difference between the surface tension of the clean interface σ_0 and that of the interface containing the surface active components at a surface coverage Γ. A_1 and A_2 are interfacial areas in two adjacent points in the curve and Π_1 and Π_2 are their corresponding surface pressures. If the compression is

slow enough and the experiment reflects true equilibrium properties, then $K_{app} \approx K_{\Pi}$ and $1/K_{\Pi}$ is the compressibility of the interface.

However, for systems such as asphaltenes the data obtained with these widely used techniques should be treated carefully, as the occurrence of extra stresses (Eq. 1) imparts a more complicated response which renders the experimental analysis more difficult. First, the interfacial tension measurement in the pendant drop device relies on shape fitting, i.e. fitting the drop shape to a solution of the Laplace equation which only accounts for surface tension. For a complex interface displaying solid-like properties, as in the case of asphaltenes, the drop shape can significantly deviate from the Laplacian shape and fitting gives values for the surface stress which can be off by factors[41]. Thus, these measurements can be used in a regime where interfacial tension dominates over mechanical stresses, but are not valid when such extra mechanical stresses become important[41–43]. A careful analysis and validity check of interfacial tension measurements and small-step deformation of an aqueous pendant drop immersed in an asphaltene solution was recently done by Rodríguez-Hakim et al.[44], where it was shown that for such soluble systems, at short times and for quasi-static deformations the Y-L equation remains valid. Second, as both thermodynamic and dilatation rheology contributions are isotropic, it is not straightforward to decouple them[43,45,46]. Also, the compression in the rectangular trough constitutes a complex deformation with the details of the deformation depending on the ratio between shear and compressional properties[45–48]. Finally, both shear and dilatational experiments are typically carried out by using an asphaltene-soluble organic (aromatic) phase, such as toluene or xylene, or partially soluble, as is the case of studies using heptol, a combination of heptane and toluene, or even diluted crude oils and bitumen. In this way, results are reported in terms of bulk solution concentrations and it can be difficult to assess the interfacial coverage under these conditions. Assessing the interfacial coverage is specially important when trying to relate measured rheological properties to other experiments, like bulk emulsification or droplet-droplet coalescence experiments. The complexity present in real systems makes the experimental observables represent different

contributions, some related to the intrinsic material behavior, and some aspects related to the transport phenomena in the specific geometry of the experiment. Here, we will focus on the thermodynamic and rheological properties for insoluble Langmuir interfaces, so that at least there is no interplay of adsorption/desorption phenomena and the intrinsic rheological material functions can be measured. As adsorption phenomena in asphaltenes are typically slow and irreversible[6], this implies that the properties of insoluble layers at a given surface coverage are relevant for processes with a short time scale, such as drop deformation, film thinning and break up. We wish to interrogate if in first order the mechanical response is dictated by the colloidal nature of the nanoaggregates with the properties being predominantly controlled by surface coverage, or if complex physicochemical interactions or molecular entanglements dominate, in which case ageing and a dependence on the chemical nature should be observed[23,36,49].

In the present work, we hence aim to resolve the question on the nature of the mechanical response of insoluble asphaltene layers. To separate changes in interfacial tension from those in rheological properties, an array of experimental techniques is used for clarifying both shear and dilatational responses. We moreover provide good control over the surface concentrations by spreading the asphaltenes directly at the interface between an aqueous phase and an asphaltene-insoluble organic phase (alkane). To interrogate the importance of nanoaggregate interactions, experiments are also carried out at the air-water surface for comparison purposes as this is expected to amplify certain attractive interactions forces acting through the air. Since it has been shown that water-in-crude oil emulsion stability is reached once the droplets are close to monolayer coverage, focus is given on dense layers since these conditions represent the most relevant ones. In addition, we evaluate how significant chemical heterogeneity is in influencing the properties of asphaltene layers by using different subfractions, as a consistency check.

Materials and Methods

Materials

Milli-Q water (Advantage A10, resistivity 18.2 MΩ.cm) was used as the aqueous phase and n-hexadecane (99% Acros Organics) as the oil phase. Hexadecane was chosen as asphaltenes are insoluble, its mutual solubility with water is quite low and it has low volatility compared to other n-alkanes. Asphaltene samples and their subfractions were prepared at the Ugelstad Laboratory in NTNU. Asphaltenes were precipitated from a North Sea crude oil by using n-hexane following the procedure described in[50]. This will be further-on referred to as the "whole asphaltenes" sample, whose results are discussed in the first part of the results section. Subfractions can be prepared in different ways[29,51–53]. In the present work, adsorption on calcium carbonate was used, as depicted in Fig.1[50]. Briefly, a solution of the whole asphaltenes in toluene is allowed to flow through a packed bed column of $CaCO_3$ and eluted with toluene. The solution collected at the bottom of the column at the end of this elution step corresponds to the first subfraction ('bulk asphaltenes'). Subsequently, the column is further eluted with chloroform, and at the end of this step the 'adsorbed asphaltenes' subfraction is obtained. The remaining asphaltenes are obtained after dissolution of the $CaCO_3$ column with a mixture of chloroform and HCl solution, and the last subfraction ('irreversibly adsorbed') is obtained from the organic supernatant.

Information about the subfractions used in this work can be found in Table 1. Molecular weights were measured by ESI(+)FT-ICR mass spectrometry as described in the work by Pinto et al.[54]. The yield of each subfraction, i.e. the mass percentage obtained after the fractionation procedure with respect to the initial mass of whole asphaltenes, is also listed. It is important to note that the so-determined molecular weight values are quite different from the widely used average value of 750 g/mol, even for the whole asphaltenes, and that the values listed represent an average of a molecular weight distribution measured for each subfraction. As will be discussed in the results, accounting for molecular weight differences

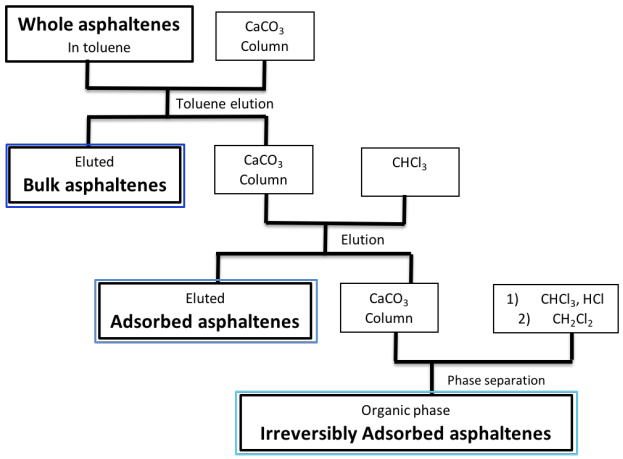

Figure 1: Column fractionation procedure used to obtain the asphaltene subfractions based on adsorption on calcium carbonate.

is very important when comparing the different subfractions. Table S1 in the Supporting Information (SI) contains elemental analysis data published by Ruwoldt et al. [50], where the exact same fractionation method based on column adsorption was used for a different batch of subfractions.

Table 1: Molecular weights[54] and yields of the individual subfractions used in this study.

	MW [g/mol]	Yield (%)
whole asph.	493	-
bulk	508	29.5
adsorbed	399	48.1
irrev. ads.	442	11.8

For all fractions, a stock solution of 1 mg/mL in toluene (VWR Chemicals, AnalaR Normapur >99.5%) is prepared. According to the colloidal aggregation picture of the Yen-Mullins model[11], at this concentration asphaltenes are present as nanoaggregates. In crude oils, asphaltenes will likely be present at concentrations higher than CNAC so we believe this to be most relevant scenario for the crude oil emulsion problem. Indeed, the most stable, and hence more problematic emulsions occurs for heavy crude oils, which are crude oils with typically high asphaltene contents.

Asphaltene interfaces are created by spreading the solution from an aliquot directly

onto the fluid-fluid interface. Before each measurement, the sample is sonicated (Bandolin Sonorex, 35kHz) for 15 minutes to ensure a reproducible state with small nanoaggregates. By adding the solution drop-wise across the entire interfacial area using a microliter syringe (Hamilton Gastight® 1700, 50μL), a uniform interfacial distribution of the asphaltenes can be achieved. The obtained mass coverage can be converted to an average 'area per molecule' (or mean molecular area, [Å^2]), with the available values of molecular weight for each sub-fraction. It is worth noting that the amount of solution spread is $\sim$ 10 µL, depending on the desired interfacial concentration and interfacial area of each set-up (troughs or DWR), which in general is negligible compared to the total volume of bulk phases ($\sim$ 10 - 100 mL). The reproducibility of the experiments confirms the adequateness of this procedure (see Figure S1 in SI).

Characterization of interfacial behavior

Figure 2 presents an overview of the techniques employed in the present work, namely the Langmuir trough for compression-expansion experiments, radial trough for dilatational/ compressional rheology, and double wall-ring for shear rheology, which are described next in detail. All devices are placed on anti-vibration tables and are enclosed in plexiglass boxes to minimize external disturbances.

Compression in Langmuir troughs

Compression experiments are carried out in rectangular liquid-liquid Langmuir troughs (360 x 55 mm) from KSV Nima (Biolin Scientific) as depicted in the first image of Fig. 2. A uniaxial compression profile occurs if a slip condition at the trough's side walls is satisfied; if this is not the case a complex mixed deformation profiles takes place, with compressional and shear components[48,55]. For stepwise compressions, a liquid-liquid trough with dimensions 784 x 75 mm was also used due to its high maximum compression ratio. Both set-ups consist of a PTFE trough with two motor-controlled Delrin barriers, a sensitive electromagnetic balance

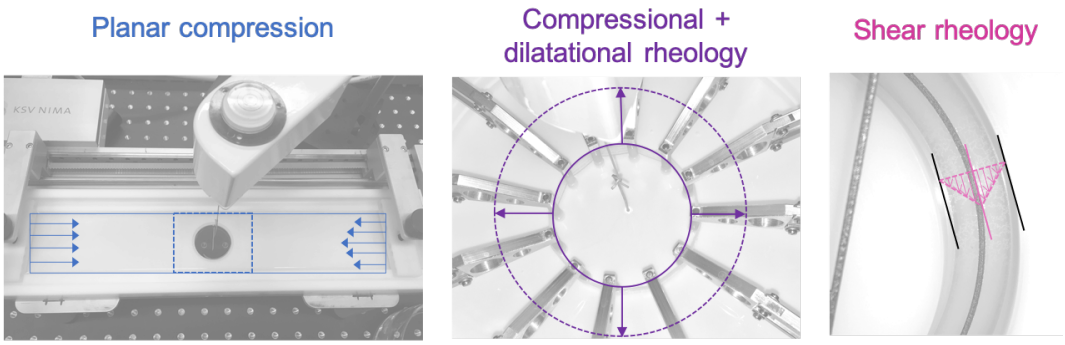

Figure 2: Overview of the techniques used to fully characterize the different contributions to the total interfacial stress (Eq. 1) and their corresponding velocity profiles. Compression in Langmuir troughs, where the profile on the left side depicts an uniaxial compression in case the slip boundary condition is satisfied, while the profile on the right depicts a slightly parabolic profile corresponding rather to a “squeeze-flow" type of deformation which might occur in the case of more structured interfaces; dilatational/compressional rheology in radial trough; shear rheology in double wall-ring (DWR) geometry.

(resolution 0.1 µN/m) coupled to a Wilhelmy plate, using a fluids bath for temperature control. The troughs and barriers are first cleaned with precision wipes (Kimtech Science) soaked with toluene, rinsed with ethanol, then wiped with detergent, and then thoroughly rinsed at least three times with Milli-Q water and ethanol. The platinum Wilhelmy plate is rinsed with ethanol and acetone, and subsequently flame-treated to remove any organic contaminants prior to all experiments.

In a typical compression experiment, the trough is filled with the aqueous subphase and the Wilhelmy plate is placed at the surface. The surface tension is checked to be 72.7 ± 0.3 mN/m. For O/W interfaces, the oil phase is carefully added to the top of the water surface until the Wilhelmy plate is completely covered. The interfacial tension is checked to be 52 ± 0.5 mN/m and a waiting time of 15 minutes is allowed for temperature equilibration. Then, a compression is carried out with the bare interface to ensure that the interface is free of contaminants. For air-water interfaces, the surface pressure should not increase above 0.2 mN/m, whereas for O/W an acceptable value for surface pressure variation upon compression-expansion would be < 1.0 mN/m. After this step, an insoluble monolayer can be created by spreading the asphaltene solution drop-wise directly at the interface with a

Hamilton μL-syringe. Again, time is allowed ($\sim$15 min) for the toluene to evaporate, in case of air-water surface, or to dissolve into the oil phase in the case of liquid-liquid interfaces. On one hand it has been shown that solvent can still be entrapped within the nanoaggregates even after long waiting times[56,57], yet on the other hand this most likely comes closer to reflecting real asphaltene interfaces, as recently argued by Samaniuk and coworkers[58]. In the end, the degree to which solvent is entrapped will mainly affect the local packing: it has been shown e.g. that while good solvents such as toluene will become more entrapped and may swell the nanoaggregates, poorer solvents will lead to denser layers[25]. All compressions were carried out at a speed of 3 mm/min and temperature of $23 \pm 0.5\,^{\circ}$C. Changing the speed of compression from 0.5mm/min to 5mm/min did not yield significant differences. One cycle consists of compressing and then expanding back the interface once, whereas multicycle experiments refers to subsequent cycles of compressing and expanding.

Interfacial dilatational rheology

A recently developed radial trough device[46,59] was used to interrogate the compressional/ dilatational rheological properties. Figure S2 illustrates its main components: a circular Teflon trough, a set of twelve motorized fingers that will control the deformation of the interface, and a Wilhelmy balance (KSV Nima) for surface stress measurements. To keep the radial symmetry, a platinum rod is used. An elastic band is placed around the 12 fingers, so that the interface to be tested will be contained in the area inside this band (see Fig. 2). For air-water interfaces this band is made out of SBS (Vreeberg BV), but due to its incompatibility with alkanes a new, custom-made fluorinated elastic band was created to expand the measurement capabilities of this device also to experiments with oil-water interfaces. Detailed information about the synthesis and production of the new fluoropolymer elastic bands can be found in the SI. Prior to each measurement we follow the calibration procedures as in ref.[46]. For all measurements, the temperature is equal to $23 \pm 0.5\,^{\circ}$C and interfaces are prepared in the same way as described for the Langmuir

trough compression experiments. Both constant speed compression/expansion experiments (1.5 mm/min) and oscillatory experiments were carried out; for the latter, one data point stems from five oscillation cycles (two conditioning cycles followed by three cycles to average the data). In the frequency sweeps, a fixed amplitude of 1% area change was applied. Analogously to shear rheology, the interfacial dilatational moduli $K^{'}(\omega)$ and $K^{''}(\omega)$ [Pa.m] are then calculated from the amplitude ratio and the phase shift between the input (motor displacement) and the output (measured surface stress) signals.

Interfacial shear rheology

Interfacial shear rheological properties are measured with a double wall-ring (DWR) geometry[60] mounted on a DHR-3 rheometer (TA Instruments). The assembly consists of a Teflon cup placed on top of the Peltier Plate for temperature control and a Pt-Ir ring geometry attached to the top part of the rheometer. The cup has a 1 mm-size step around the inner walls to create a planar surface and the ring has a diamond-shaped cross section to enable more precise pinning of the interface. Cleaning and sample loading is similar as for the Langmuir trough experiments. All tests were conducted at 23±0.1 °C, as checked by a thermocouple. Both oscillatory (i.e. time, frequency, and strain amplitude sweeps), and creep-recovery tests were carried out. A fixed strain amplitude of 0.02%, which is well within the linear viscoelastic regime, was used for the time and frequency sweeps, whereas a fixed frequency of 2 rad/s was used for the amplitude and time sweeps. With these parameters the torque values are sufficiently high to ensure reliable data. For all oscillatory frequency and amplitude experiments, we acquire data with three conditioning cycles followed by three sampling cycles. To measure the temporal evolution in oscillatory time sweeps, 1 cycle conditioning followed by 1 cycle sampling was used. Rotational (precision, 3 iterations) and oscillatory mappings at the relevant amplitudes and frequencies are carried out, and the transducer mode is set to 'soft'. The method by Renggli *et al.* was used to ensure we were within the operating windows of the device[61].

Results and Discussion

First, results for the whole asphaltenes at both water-air and water-oil interfaces are reported. Although the most relevant case for the crude oil emulsions is that of oil-water interfaces, the air-water interface also provides insights as it changes the interactions. Then, the thermodynamic and rheological properties for the different subfractions are compared to the results for whole asphaltenes to evaluate the role of the chemical nature in controlling these properties.

Throughout the paper we will refer to surface coverage mostly in terms of area coverage (or mean molecular area, MMA [Å^2]). As will be shown, this is specially important for the second part of the results because it enables a better comparison between different subfractions that have different molecular weights as opposed to comparisons made on the basis of mass coverage. Of course, based on the concentration of the spreading solution, asphaltenes are present as nanoaggregates in our measurements and not as single molecules. Orbulescu et al.[57] used solutions with the same concentration as ours for Langmuir trough experiments and have shown that asphaltenes remain as nanoaggregates when spread at the air-water surface using Brewster angle microscopy. In the present work, the MMAs are calculated based on the available molecular weight values (see Table 1), and hence the absolute values likely do not reflect the actual area being occupied by the nanoaggregates at the interface, but still give a "first order" measure of area coverage. Nonetheless, if a higher "nanoaggregate weight" would be available, this difference would represent a shift in the x-axis towards larger MMA, so that the observed trends would still be the same. The complex and heterogeneous nature of asphaltenes renders it difficult to think about a single value to characterize their size. In fact, NMR studies with an asphaltene solution at the same concentration used here shows a distribution of nanoaggregate sizes with hydrodynamic radius ranging from 5 - 60 Å[62]. This polidispersity would shift in maximum packing to slightly higher values. In a recent study using microrheology[63], asphaltene interfaces were shown to be spatially heterogeneous on a μm scale, which might indeed be due to differences in sizes

of the nanoaggregates adsorbing at the interface. Still, we opted here for plotting all data in terms of area coverage since packing seems to be the key parameter when interrogating these interfaces.

Whole asphaltenes

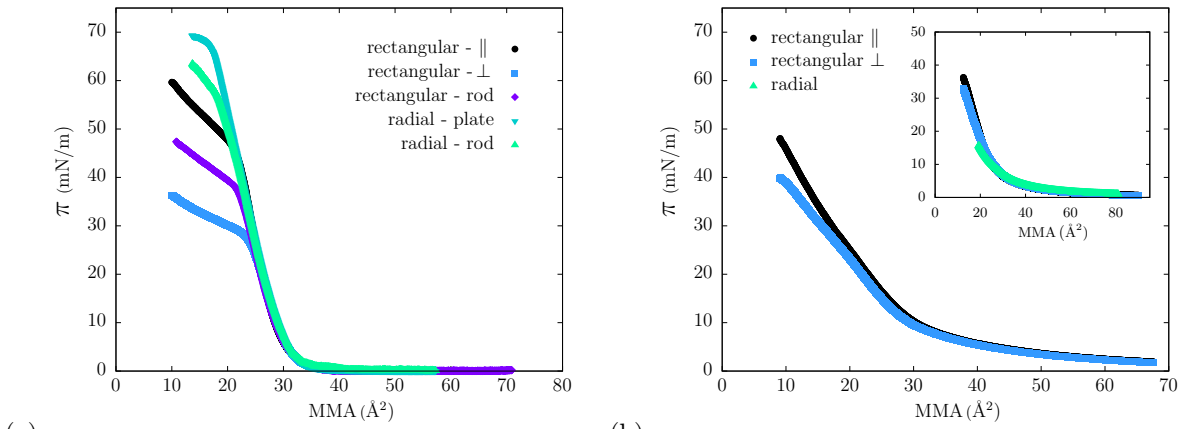

Figure 3: Compression experiments of the whole asphaltenes at (a) air-water surface and (b) oil-water interface. Comparison between different plate orientations, in the rectangular Langmuir trough, i.e. ∥ and ⊥ with respect to the barriers, and isotropic compression in radial trough. Inset in (b) shows compression starting at higher mean molecular areas.

Indigenous asphaltene nanoaggregates were spread and compressed in both rectangular and radial Langmuir troughs. Figure 3 shows the experimentally measured surface pressure Π as a function of area per molecule for the (a) air-water and (b) for oil-water interfaces. For the air-water surface, the surface pressure is close to zero for a wide range of the compression until an area per molecule of about 33 Å^2 is reached, when Π starts to increase very steeply. Around 20 - 25 Å^2 slope changes occur at distinct surface pressures, which however depend on the measurement geometry used. What is perhaps most striking in this plot is the difference between results obtained with different probe orientations but only below a certain area per molecule. What is being measured is hence not a thermodynamic state variable, which should only depend on Γ and T, and the differences can be attributed to extra and deviatoric, mechanical stresses. This has also been shown for different types of structured surfaces, as

e.g. those populated by carboxylic acids[64] and for acrylate polymers[46] at air-water interfaces. For this reason we do not refer to these plots as isotherms, but rather as compression curves.

By comparing the results pertaining to the rectangular trough (black, purple and dark blue curves), we see that the parallel-oriented plate presents a change in slope at much higher Π values than the one oriented perpendicularly with respect to the barriers. This is because the deformation field has both shear and compressional components and thus different plate orientations pick up different stresses[45,48,55,65], implying that the layer at the water-air interface has a significant shear modulus, i.e. it is a displaying solid like behvaiour. The inflection point at high surface pressure corresponds to a point where transparency of the surface layer is reduced due to the formation of structures, namely dark stripes that can be seen by the naked eye and that are parallel to the barriers in the case of the rectangular trough. This is wrinkling and buckling of the asphaltene nanoaggregate monolayer, consistent with previous studies using Brewster angle microscopy (BAM) experiments[66,67] and more recently with interference reflection microscopy (IRM)[58]. Results for the compression in the radial trough (light blue curves) present similar behavior during compression, however buckling occurs only at a much higher surface pressure and the dark stripes on the interface show no preferential direction due to the purely isotropic nature of the compression. Recently, Fajardo-Rojas et al.[58] also compared compression measurements of asphaltenes at air-water surfaces in both rectangular and a radial trough. In contrast to our results, they found significant differences between both devices already from the beginning of compression, which they attributed to the difference between isotropic vs. mixed deformation modes. However, the present data show that this does not seem to be the cause; rather, this is possibly due to a difference in initial conditions between their experiments, i.e. different initial coverage and non-zero initial surface pressure in the radial trough.

The results for the oil-water interfaces in Fig. 3b are more featureless. The surface pressure increases steadily during the compression with a small inflection at around $30\,\text{Å}^2$, and the parallel-orientated plate leads to only slightly higher surface pressure values at high

compression. The inset shows a comparison between the rectangular and radial troughs at smaller coverages. Due to the smaller maximum compression ratio of the radial trough compared to the rectangular trough, it is not possible to cover the same range in mean molecular area (MMA). Indeed, the differences observed between different plate orientations are small compared to the differences seen in Fig. 3a, but the curves diverge at approximately the same surface coverage as observed for the air-water layer. Interestingly, no macroscopic buckling is observed at the range investigated. This suggests that no out-of-plane deformation occurs at this point and that a different and smoother rearrangement takes place. Since it is very unlikely that asphaltenes desorb to either bulk phases, one possible mechanism for stress relaxation can be multilayer formation of nanoaggregates. It has also been previously suggested[20] that the 'skin formation' observed in pendant/rising droplets occurs due to multilayer formation, either due to very long adsorption times and consequent accumulation at the interface or due to compression of the asphaltene monolayer.

This difference in behavior upon compression observed in Figs. 3a and b is most likely due to the difference in the nature of interactions at air-water vs. oil-water interfaces, where both subphase-asphaltene and asphaltene-asphaltene interactions play a role. At the air-water surface the carboxyl groups have affinity to the water phase but the alkyl chains have no affinity for air, so that stronger (lateral) interactions are present. Conversely, at oil-water interfaces the hydrophobic chains have affinity for the top oil phase, and hence asphaltenes are expected to interact less with each other. Moreover, the Van der Waals forces acting across the air can be expected to be stronger compared to having oil as the top phase due to higher dielectric constant of the latter. This is also the cause for difference in compressibility for the two types of layers, namely that asphaltenes at air-water interfaces present lower apparent compressibility in accordance with previous studies[68].

It should be noted that the maximum surface pressure for water is $\Pi \approx 72$ mN/m and 50 mN/m for alkane-water interfaces, which implies that asphaltenes are not very surface active when thinking about their ability of lowering the energy of the surface. They only

reach higher surface pressures when compressed. Measured values (see Fig. S4) of the equilibrium surface pressure of the oil-water interface are around 5-15 mN/m, in agreement with literature values[69,70]. What we are measuring in these compression experiments, in the case of complex, structured interfaces, is the total surface stress σ, and not just $\sigma_{\alpha\beta}$.

It is useful to compare the interfacial coverage where solid-like behavior and extra stresses occur with the reported minimum mass coverage for emulsion stability, which are reported to be in the range of 3 - 5 mg/m^2 for different crude oils[28,71,72]. Works using North Sea crude oils are taken as a reference, specifically for the excess surface coverage (Γ_∞ = 4.0 mg/m^2) from adsorption studies[73] and a value of critical mass coverage for coalescence (Γ_{crit} = 3.5 mg/m^2)[28]. These two values differ in the sense that while the former represents a value for monolayer coverage of the interface, the latter represents a minimum coverage for coalescence suppression, which has been shown to occur even below monolayer coverage. By plotting the same data as in Fig.3a as a function of mass coverage (Fig. S3), we observe that the curves between different geometries start to deviate (indicating the onset of strong mechanical stresses) at around this Γ_{crit}, and that the interface buckles under uniaxial compression at values close to Γ_∞ and slightly higher for isotropic compression.

Cycling the pressure-area diagrams provides insight into the nature of the interactions between the species and aggregation behavior, as it interrogates the reversibility of these interactions. Figure 4 presents results for (a) air-water as well as for (b) and (c) oil-water asphaltene interfaces with very distinct responses. Filled lines indicate compression and dashed lines indicate expansion. In Fig. 4a for the air-water surface, after the first compression the surface pressure drops immediately back to 0 and remains so during the entire expansion, indicating a (brittle) fracture where connectivity is lost immediately upon expansion. During the second compression, the surface pressure rises slightly more steeply to essentially the same maximum compression but only close to maximum compression, in agreement with an interface that has cracked upon opening, without re-spreading, but percolating again when the fractures interlock. The maximum surface pressure varies from 65 mN/m in the first cy-

cle to 58 mN/m for the third one, indicating that maybe some material is lost upon buckling or an overlap is created.

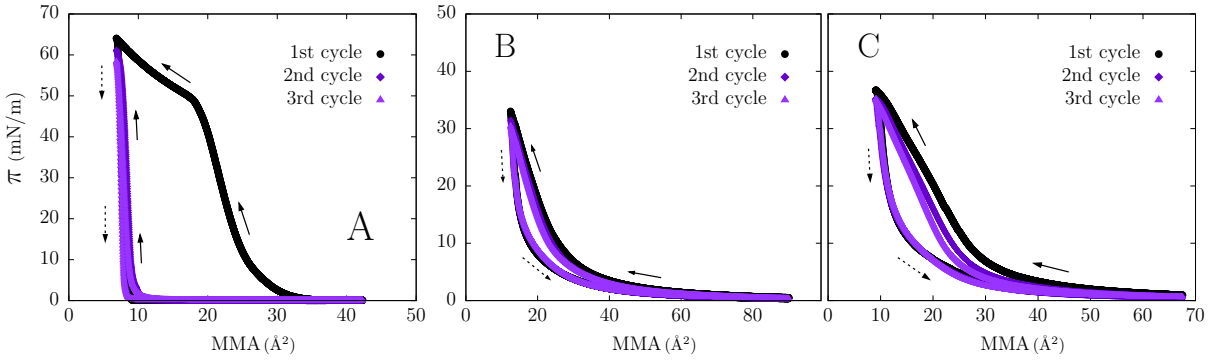

Figure 4: Multicycle compression-expansion experiments in the Langmuir trough of whole asphaltene at (a) the air-water surface; (b) and (c) at oil-water interfaces starting at different initial surface coverages.

The behavior of the oil-water interface is qualitatively different. In Figure 4b we see that all three cycles have the same general behavior, displaying only some hysteresis and very little changes between the subsequent cycles. Moreover, variations in maximum surface pressure reached upon compression are negligible and the same surface pressure is obtained when expanding back to maximum interfacial area, so no material is lost to the subphase. All these observations are consistent with the formation of a densely packed layer, where no irreversible aggregates are formed and the hysteresis most likely stems from in-plane relaxation phenomena. When the initial coverage is slightly higher (Fig. 4c) more pronounced hysteresis and differences between the cycles observed. This is an indication that at these lower MMA asphaltenes aggregate more irreversibly. As in this case we are compressing beyond what is assumed to be nanoaggregate monolayer coverage, multilayer structures can be formed at the interface, which are only partially reversible. Lin et al.[74] have indeed shown that at mass coverages around a few mg/m^2 an homogeneous layer is seen, but at very high coverages μm-sized multilayer aggregates could be observed. This suggests that above a certain packing state different dynamics and interactions come into play at the o/w interface, as will be confirmed also from the experiments presented next.

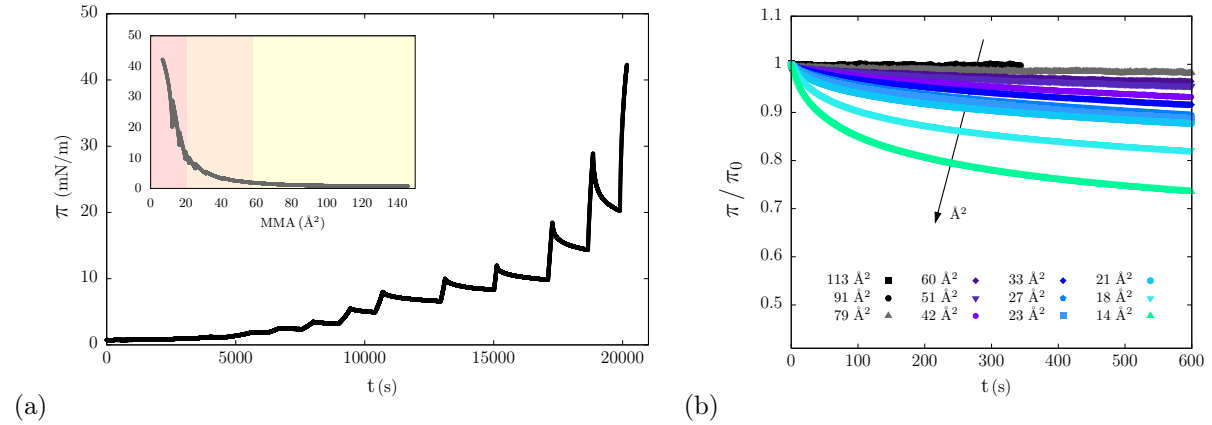

(a) (b)

Figure 5: Stepwise compression of asphaltenes at the oil-water interface in the Langmuir trough: (a) surface pressure vs. time, with inset Π vs. area, (b) normalized individual relaxation steps.

Having established that no desorption occurs, stepwise compressions can be used to assess the relative magnitudes of the thermodynamic vs. viscoelastic contributions to the total stress. Figure 5a contains results for a stepwise compression experiment at the oil-water interface plotted as a function of time, and in the inset the same experiment as a Π-area per molecule diagram. Figure 5b displays the normalized individual decays. For the initial, lower coverages in the yellow shaded area of the inset plot (MMA $> 60\text{Å}^2$) there is no relaxation as surface tension changes control the behaviour. However, as the surface coverage is increased upon further compression, relaxation gradually starts to be observed, becoming more pronounced with increase in surface coverage. Indeed, two distinct viscoelastic relaxation regimes can be observed: one, at intermediate area per molecule ($\sim$58 to 22Å^2) indicated by the orange shaded area, where relaxation takes place and surface pressure values relax to up to 25% of their original value, and a region highlighted by the red shaded areas where the stress relaxes about 30 - 45%. This means that at these coverages a significant part of the measured surface stress in a continuous compression curve is certainly viscoelastic. The stress decays in the intermediate coverage region can be well fitted with a stretched decay exponential function

$$\Pi\left(t\right) = \Pi_{eq} + a\, e^{(-t/\tau)^{\beta}} \tag{4}$$

where Π_{eq} is the equilibrium value of surface pressure, τ is the relaxation time, and β is a dimensionless exponent. When $\beta < 1$ this indicates the presence of wide distribution of relaxation timescales. This occurs in a range of mean molecular areas consistent with a dense layer but still below assumed monolayer coverage. At the highest coverages, the stress relaxation data is better fitted by a double exponential decay function with two relaxation times, τ_1 and τ_2 which are the short- and long-mode relaxation times. Examples of the fits are shown in Figure S5. From the results it can be concluded that the in-plane relaxation is slow, on the order of 10^2 - 10^3 seconds. Comparing the magnitude of the relaxation times τ, to timescales of typical processes for emulsions t_p (e.g. flow or mixing), defines the Deborah number $\mathrm{De} = \tau/t_p$. When the process time scale is small compared to the relaxation time scale, the asphaltene interface can be treated as an elastic interface. Specifically, for the coalescence problem, where the droplet collision occurs at short timescales ($\sim$ seconds), De will be at the order of 10^3, meaning that these interfaces will behave highly elastically. From the comparison to a continuous compression curve (data not shown here - see Fig. S6) it can be seen that even though the surface pressure values decay by a significant amount upon relaxation, as soon as the interface is further compressed the same surface pressures are reached. This shows that the viscoelastic relaxation taking place is effectively an in-plane relaxation, and no material is lost from the interface.

The underlying isotherm can be constructed from the Π_{eq} values obtained after relaxation of the mechanical stresses as shown in Fig. 6 and fitted with the Volmer equation of state[75], which has been shown to capture the behavior or insoluble monolayers of nanoparticles at interfaces[76,77]:

$$\Pi = -\frac{k\,T}{w_0}\left[\ln\left(1 - \frac{w}{A}\right) + \left(\frac{w}{A}\right)\right] - \Pi_{coh} \tag{5}$$

where k is the Boltzmann constant, T is the temperature, w_0 the area occupied by a molecule of the subphase, w the area covered by the particles, A is the total interfacial area, and Π_{coh} is the surface pressure of cohesion, which is related to the interactions between the particles

at the interface. For this experiment, the actual total area covered by the asphaltenes is $w = 73.3\,\mathrm{cm}^2$ as calculated from the amount spread and the MMA discussed above, which agrees well with the w obtained with the fit. In addition, the calculated w_0 is consistent with the size of water molecules ~ 0.2 nm^2. These two values are taken as an indication to assess the quality of the fit.

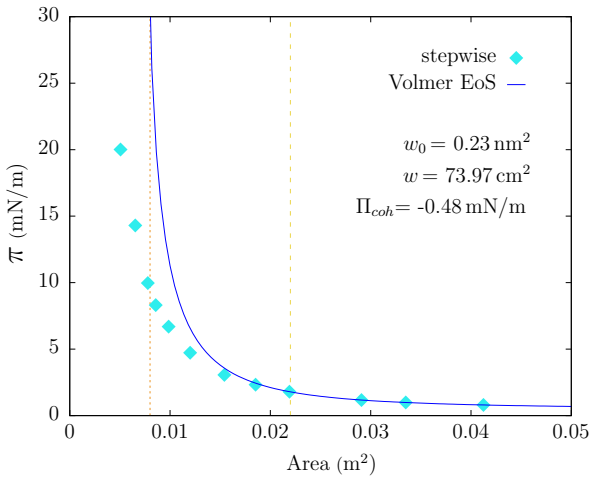

Figure 6: Isotherm of whole asphaltenes at the oil-water interface fitted with the Volmer equation of state. Yellow and orange vertical dashed lines indicate coverages corresponding to the apparent onset of the different regimes as depicted in Fig. 5.

A reasonable quality fit could be obtained up to the point where solid like interfacial behaviour emerges (A $\sim$ 0.02 m^2, which corresponds to a MMA of 50Å^2). Surface pressure values do not exceed 20 mN/m, in agreement with typical reported values for equilibrium interfacial tension. Still, there are likely some residual mechanical stresses in the values of Π_{eq}, specially at high coverages. Thus, we again see evidence that asphaltenes are not very efficient in lowering surface tension. Also, from the rather small values of Π_{coh}, it seems that the nanoaggregates do not interact strongly, even showing a slightly repulsive behavior. As a comparison, for attractive species at the interface, as e.g. graphene oxide[76] or rough carbon black particles[77] which undergo strong lateral capillary interactions, Π_{coh} values ranged from 6 - 9mN/m up to 12mN/m, respectively. For the air-water surface, a fit with the Volmer equation (Fig. S7) yields positive values of Π_{coh} indicating again the

attractive nature of interactions.

Interfacial dilatational rheology

Obtaining the EOS is also important for subsequently studying and analyzing dilatational rheology data. The value of K_{Π} can be compared to $K^{'}$ to assess the relative contributions of the compressibility and the extra stresses. Following this rationale, Fig. 7 presents $K^{'}(\omega)$ and $K^{''}(\omega)$ at an area strain amplitude of 1%. Surface concentrations shown represent distinct cases, namely that of a 'weak' interface (50 Å^2), a densely packed, close to monolayer coverage one (21 Å^2) and an interface that likely has already assembled in multilayers at the oil-water interface (13 Å^2). For the air-water interface, only the second scenario was studied, because at 50 Å^2 surface pressure is essentially zero, and at 13 Å^2 the interface has already buckled and hence would lead to out-of-plane deformations. The dashed lines correspond to values of K_{Π} calculated with Eq. 3 from the EOS, and at high coverages where the EOS diverges, from the equilibrium data points in Fig. 6.

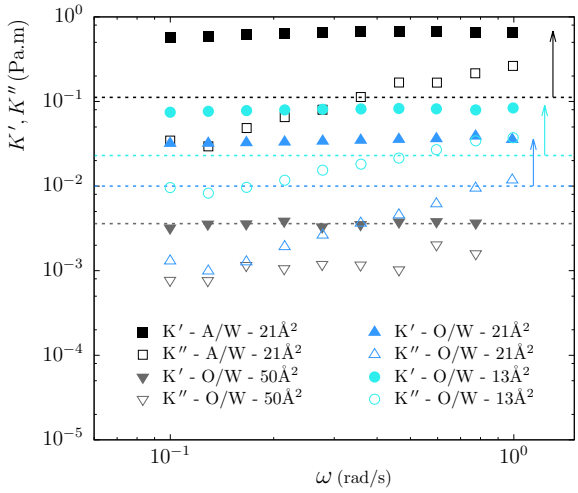

Figure 7: Dilatational frequency sweeps at different surface coverages and comparison to the static elasticity K_{Π} (dashed lines) obtained from stepwise compression experiments. Arrows highlight the difference between the thermodynamic (Gibbs elasticity) and mechanical contributions to the measured elastic modulus.

For all cases K' is relatively frequency-independent, $K' \sim \omega^n$ with n < 0.1, and the

total elastic contributions is larger than the viscous one ($K^{'} > K^{''}$). For the largest area per molecule $K^{'}(\omega)$ is equal to K_{Π}, indicating that the dilatational response is governed by the compressibility, in line with the observations of the previous section that for these concentrations the response is that of a simple interface. With increasing coverage, the extra stresses due to the emergence of a solid-like structure come into play and $K^{'}(\omega) > K_{\Pi}$, as indicated by the arrows. Also, comparing the moduli measured for air-water surfaces, where mechanical stresses are more pronounced, we observe those to be one order of magnitude higher when compared to oil-water interfaces, which is consistent with the picture of a more strongly interacting, aggregated interface (see Fig. 4).

Interfacial shear rheology

Shear rheological measurements enable us to further interrogate the structure and dynamics of the solid interface at a given surface concentration. Figure 8 shows an oscillatory time sweep conducted upon asphaltene spreading at the oil/water interface. Here, the time evolution is presented in terms of the interfacial shear elastic modulus $G_i^{'}$ (filled symbols) and interfacial shear viscous modulus $G_i^{''}$ (empty symbols). Every subsequent shear rheological experiment presented later on is preceded by a time sweep like this one as a way to ensure that we start always from reproducible conditions.

Figure 8 shows how the moduli develop during the creation of the insoluble interface. The moduli start out below the resolution of the DWR. At t = 30 s asphaltene incorporation occurs and at this moment data looks very scattered, probably because the flow fields inside the gap are disturbed by the spreading, which takes approximately 60s. Shortly after 100s, the moduli start to increase, with $G_i^{'}$ becoming larger than $G_i^{''}$ almost immediately, evidencing the formation of a structured interface. Soon after, both moduli become constant and remain so, as highlighted by the inset plot. It is worth pointing out the magnitudes of the measured viscoelastic moduli: $G_i^{'}$ is $\mathcal{O}(10^{-2})$Pa.m, and by estimating an interfacial thickness of ~ 10 nm as measured from SANS experiments[25,78,79], this would correspond to a bulk modulus of

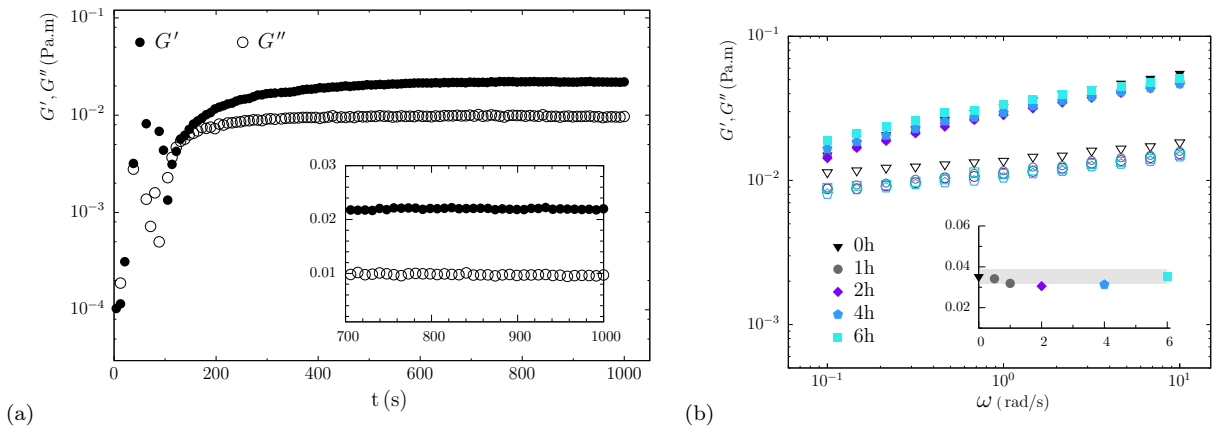

Figure 8: Oscillatory time sweep (γ_a=0.02%, ω= 2 rad/s) for a liquid-liquid interface to illustrate the creation of an asphaltene dense layer (20 Å^2). The inset plot shows the last 300s of the experiment in linear scale for the y-axis. Spreading occurs at t = 30 s; (b) A sequence of frequency sweeps (γ_a=0.02%) performed up to 6 hours after spreading also show no significant time effects for the Langmuir interfaces obtained by spreading. The inset summarizes the values of G_i^* (for ω= 1 rad/s) as a function of time. The grey-shaded area reflects changes in ±10% with respect to the initial value.

$\mathcal{O}(10^6)$Pa, indicating how strong these interfaces are.

Interestingly, no indication of "ageing" effects are seen for these model, insoluble asphaltene nanoaggregate layers, as opposed to many studies in literature where ageing is still observed after hours. This is often attributed to physical crosslinking at the interface[4,22–25,36–38,49]. The absence of ageing is however clearly evidenced by the data in Fig.8(b), where a sequence of frequency sweeps performed for up to 6 hours after spreading shows no significant time evolution of the moduli. Verruto et al.[49] showed that when ageing is present the timescale for evolution of the moduli can depend on pH and ionic strength, whereby the authors observed a "delayed film consolidation" (order of several hours) when salt in present in the aqueous subphase, and that increasing ionic strength leads to an increasing delay in consolidation; they have attributed this to asphaltene nanoaggregates having dissimilar charges and the attractive electrostatics being screened by the addition of salt. For our spread interfaces, no delay in the evolution of the moduli was observed when using a brine (∼0.6M NaCl solution) aqueous phase (see Fig. S8). In the work by Harbottle et al.[38], where also Milli-Q water with unadjusted pH 5.5 was used as the subphase, a 2-order of magnitude

increase in the moduli in a timescale of 4.5 hours is observed both for soluble (toluene) and partially soluble (heptol) oil phases. The absence of time effects in the insoluble layers presented here shows that the ageing observed in other works must be due to aspects related to adsorption from the bulk phase and solubility in the oil, either due to variations in surface coverage or due to a more complicated interfacial structure, possibly caused by multilayers or a more swollen state of the aggregates. It has been observed for some systems that the adsorption of asphaltenes follows an initial fast, diffusion-governed adsorption [69,80,81], which could be due to adsorption of the first layer containing more polar components, followed by a slower adsorption step and possibly multilayer formation [20]. Indeed, it has been shown (from QCM-D experiments) [38] that layer thickness increases over time. Moreover, higher bulk concentrations lead to a faster "build-up of a network" at the interface, which is possibly related to faster adsorption dynamics; or conversely, at a given ageing time, an interface created from a with higher bulk concentration will display higher moduli because it is more populated. In studies where high concentrations of asphaltenes are used combined with partially-soluble oily bulk phase (e.g. heptol), in addition to these adsorption effects also the occurrence of flocs might explain the ageing as inferred from rheology, as flocs have been observed to grow over time in contrast to nanoaggregates. Spontaneous emulsification, which occurs at water-toluene or diluted crude oil interfaces [82,83], could also lead to an increase of the (apparent) interfacial moduli.

As the moduli do not change over time also enables us to reliably interrogate the intrinsic frequency- and amplitude dependency of these asphaltene-laden layers for a given area fraction. Figure 9 presents results for (a) oscillatory frequency sweeps and (b) strain amplitudes carried out at different surface coverages. In Figure 9(a) it can be seen that for the lowest surface coverage, i.e. biggest mean molecular area of 40 $Å^2$, G_i' and G_i'' are approximately equal and constant, showing the onset of weak viscoelastic behavior at coverages consistent with the ones observed in the compression experiments. For all the higher coverages, G_i' is higher than G_i'' for the entire frequency range investigated. As the surface coverage is

increased, the magnitude of the moduli increases and the phase angle decreases. Also, it is seen that the moduli display a (weak) frequency-dependent behavior for all coverages.

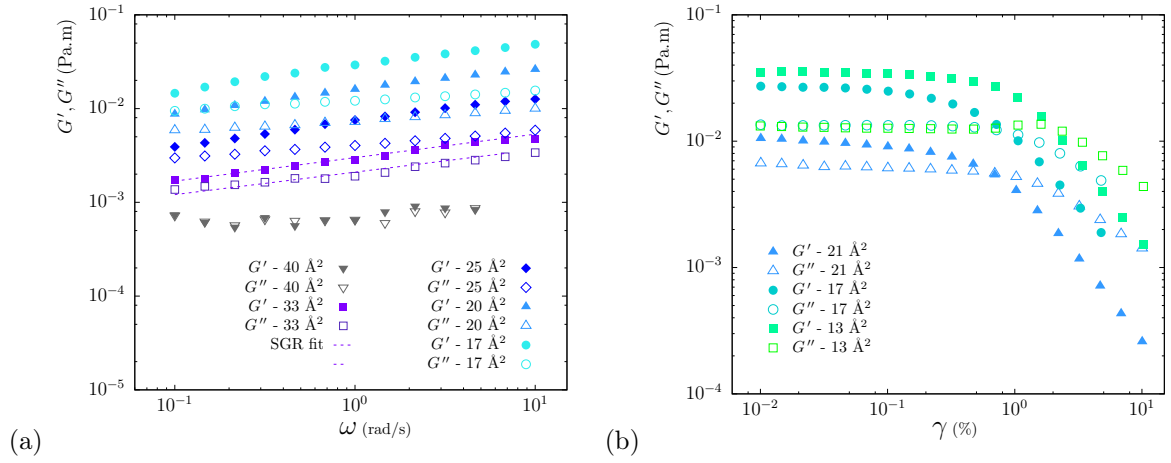

Figure 9: Oscillatory (a) frequency sweeps (γ_a=0.02%) and (b) strain amplitude sweeps (ω= 2 rad/s) performed at different surface coverages of whole asphaltenes at the water-hexadecane interface.

Following Samaniuk et al.[27] this weak frequency dependence can be captured by the soft glassy rheology (SGR) model[84–86].The main features this model describes are structural disorder and metastability for dense systems, where structural rearrangements are difficult and relaxation processes are bound to be slow. Under oscillatory flows in the linear viscoelastic regime, the SGR predicts the complex modulus to depend on frequency with:

$$\frac{G_i^*(\omega,t)}{G_{i,p}} = 1 - \frac{1}{\Gamma(x)}(i\omega t)^{x-1} \tag{6}$$

In Eq. 6, $\Gamma(x)$ is the gamma function, with x a noise temperature. $G_{i,p}$ is the interfacial elasticity of the building blocks. The effective noise temperature x dictates the rheological response: for $x > 3$, the material shows Maxwell type of behavior, i.e. viscoelastic liquid with a single relaxation time. For most materials, x lies between $1 < x < 2$ and shows viscoelastic and shear-thinning behavior, and for very dense systems $x < 1$ and the material is said to be at a glassy state. Looking in detail at the power law behavior in the frequency dependency, it is seen that for 33 Å^2 a fit with the SGR model yields $x = 1.23$, which is similar to the values obtained by Samaniuk et al.[27] for compressed asphaltene interfaces (20 mN/m). However,

the slopes of the moduli on log-log plots are seen to be no longer parallel when the coverage is increased : while the slopes of $G_i^{'}$ are approximately constant, the slope of $G_i^{''}$ decreases with increased mass coverage. The relaxation behavior is shifting from a broad SGR distribution of timescales to a more defined and slow relaxation at $\sim 1/\omega$ being in the $\mathcal{O}(10^2 - 10^3)$ s.

From the strain amplitude sweeps in Fig. 9b, the onset of a different response at coverages beyond the assumed monolayer coverage of 20 Å^2 becomes even more evident. It can be observed that at 21 Å^2, $G_i^{'}$ is only slightly higher than $G_i^{''}$' and the limiting strain amplitude is around 0.1%. As the surface coverage is further increased from 17 Å^2 to 13 Å^2, the interface becomes increasingly elastic as evidenced by the increase in $G_i^{'}$, while $G_i^{''}$ remains essentially the same. Also, the limiting strain increases to almost 1% and the bump in $G_i^{''}$ immediately beyond this strain suggest networks that dissipate energy upon breaking, which is characteristic of yielding of gels[87,88]. Consistent with the observations of the compression experiments, asphaltenes can display a spectrum of behaviours depending on the surface coverage, ranging from a simple interface with no significant viscoelasticity over a dense soft glassy layer to the presence of multilayers, though no sharp transitions are observed. Results for a/w interfaces are displayed in Fig. S9 and show higher moduli and smaller liming strain, as has been previously reported in literature[74], consistent with the picture of a more strongly aggregated and brittle interface.

To demonstrate the emergence and presence of solid-like behaviour we performed creep-recovery experiments. These tests consist of applying a constant stress step for a certain amount of time and then setting the stress back to 0 to allow for relaxation of the material. Results are presented here in terms of interfacial compliance J_i, which equals $\gamma_s(t)/\sigma_s$, as a function of time, and each color represents one creep step ($0 < t < 600$s) followed by one recovery step ($600\text{s} < t < 1200$s). Figure 10 presents results for an interface at a coverage consistent with gel-like behavior and the value of the interfacial shear yield stress is estimated to be between 2.5 and 4.0 x 10^{-4} Pa.m. For complex materials whose behavior

is also time-dependent, as most elasto-viscoplastic materials are, estimated values for this critical stress can depend on observation time. In our experiments 600s was used for the creep step, which is much longer compared to coalescence time scales in emulsions which is typically on the order of a few seconds. Also, it is important to note that the shear yield stress is one contribution to the total yield stress tensor, as has been recently discussed for bulk rheology as well[89,90]. The dilatational/compressional yield stress is more difficult to measure, even for bulk rheology, but is reported to be several times higher than the shear counterpart.

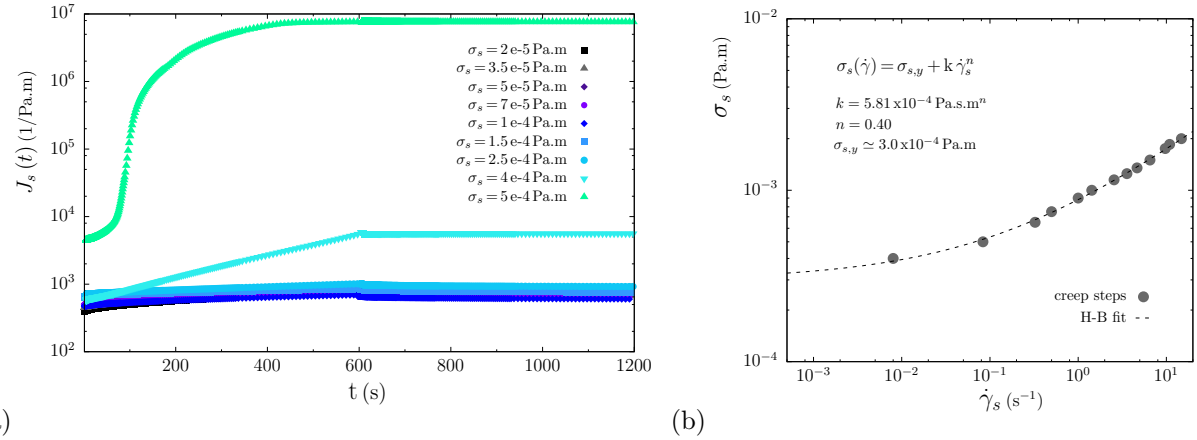

(a) (b)

Figure 10: (a) Creep-recovery test of whole asphaltenes at the oil-water interface for estimation of shear yield stress, (b) flow curve constructed from creep steps, including a fit with the Herschel-Bulkley model.

A flow curve can be constructed from steady-state values of stress vs. shear rate from the creep steps at higher stresses as depicted in Fig. 10b. Beyond $\sigma_{s,y}$ a clear shear-thinning behavior is seen. Combining these two features with the existence of a yield stress leads to the scalar Herschel-Bulkley constitutive model for describing the shear rheological response:

$$\sigma_s = \sigma_{s,y} + k\,\dot{\gamma}_s^n \tag{7}$$

where $\sigma_{s,y}$ is the interfacial shear yield stress, k the consistency index, and n the power-law exponent. We see that the fit with the Herschel-Bulkley equation agrees well with the data

and gives a shear yield stress of $\sim 3 \times 10^{-4}$ Pa.m, which is within the range estimated above. This value is in the same order of magnitude as the yield stress for dense particle-laden interfaces of spheres[91].

To interrogate the yielding behavior at lower coverages in more detail, we investigate time-stress superposition, which is a signature of glassy behavior as observed for polymers (see e.g. Tervoort et al.[92]). Time-stress superposition can be verified by shifting the creep compliance curves for different stresses. A mastercurve can be obtained if the shift factors follow a given function which is related to the stress-dependency of relaxation times in the material, i.e. $a_s = a_s(\sigma)$. For simple glassy materials the behavior is captured by the Eyring equation, but in principle other stress-dependent relations could be valid.

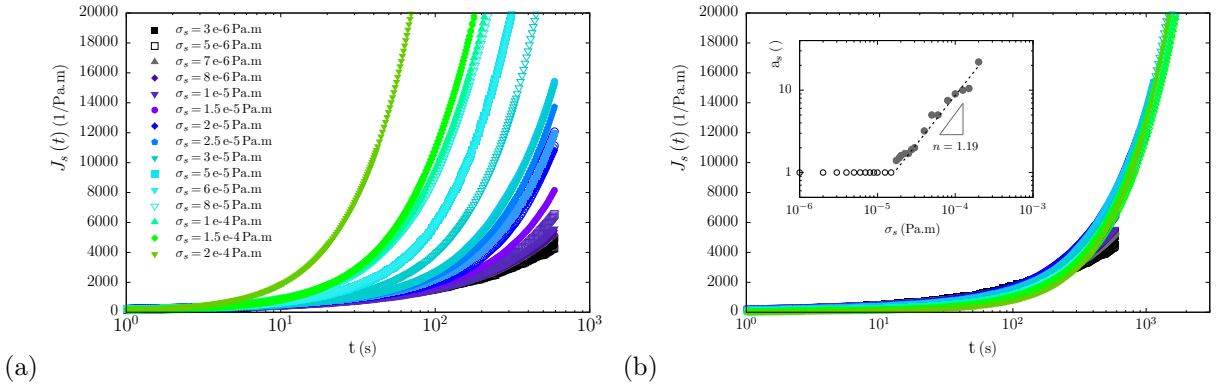

Figure 11: (a) Creep compliance curves of whole asphaltenes at the oil-water interface and (b) same data, but horizontally shifted with a_s to obtain a mastercurve. The inset plot in (b) shows the shift factor as a function of applied stress σ_s.

In Figure 11 we plot the compliance curves as $J_s = (\gamma_s(t) - \gamma_i)/\sigma_s$, where γ_i is the initial strain value at each creep step, as a function of time. Fig.11a contains the data without shifting and Fig.11b after shifting the curves horizontally. The inset plot in Fig.11b displays the shift factor a_s as a function of the interfacial stress. At the smallest applied stresses, linear viscoelastic behavior is probed and all curves overlap without further shifting ($a_s = 1$, empty symbols). As the stress is increased, the response becomes non-linear and higher a_s are needed to overlap the curves. For our asphaltene interfaces, we find that a power-law relation with an exponent ~ 1.2 describes well the data in this regime, again confirming a

distribution of relaxation timescales, in accordance with the SGR model. In contrast, for gel-like interfaces a more abrupt transition between nonlinear viscoelastic and plastic flow is observed[88].

In this section, we have obtained a complete overview of the surface concentration dependence of the interfacial behavior of asphaltene nanoaggregate Langmuir layers. The results can be summarized in Fig. 12 in terms of the magnitudes of the different moduli measured at the water-hexadecane interface in the different devices as a function of surface coverage. Taking an estimated value for nanoaggregate monolayer coverage of MMA $\sim$ 21 $\pm$ 2Å^2 following the discussion of Fig. 3, the area fraction ϕ_{area} is calculated as this value divided by the MMA of the given experiment. Here we plot the apparent compressional modulus K_{app} from the compression in the rectangular Langmuir trough using Eq. 3 (smoothed data), the Gibbs elasticity stemming from the change of interfacial tension K_{Π} (discrete points extrapolated to a continuous curve), the complex dilatational modulus from the oscillatory measurements $K^*(\omega)$, and the complex shear modulus $G_i^*(\omega)$. Both rheological moduli values were taken at a strain amplitude in the linear viscoelastic regime and $\omega = 1$ rad/s, and error bars indicate the range of observed frequency-dependency. At the highest coverage, the low value of G_i^* as compared to the dotted trend line is likely because of the nature of the interface created by spreading, as opposed to the other devices where layers were compressed to the given coverage.

First, the independently measured shear and dilatational moduli become significant at the same point the apparent modulus increases beyond the value of the Gibbs elasticity. As the surface coverage is increased the rheological contributions start to dominate over the thermodynamic ones, and beyond $\phi_{area} \sim 1$, $K^*(\omega)$ and $G_i^*(\omega)$ increase significantly. The magnitude of the dilatational moduli is higher than that of the shear moduli, suggesting that the interface is less resistant to shear than to compression. Calculating a Poisson ratio for 2D materials at this coverage with $\nu = K - G \,/\, K + G$ [41] yields a value of 0.25 for dense layers at the oil-water interface and 0.48 for the air-water interface.

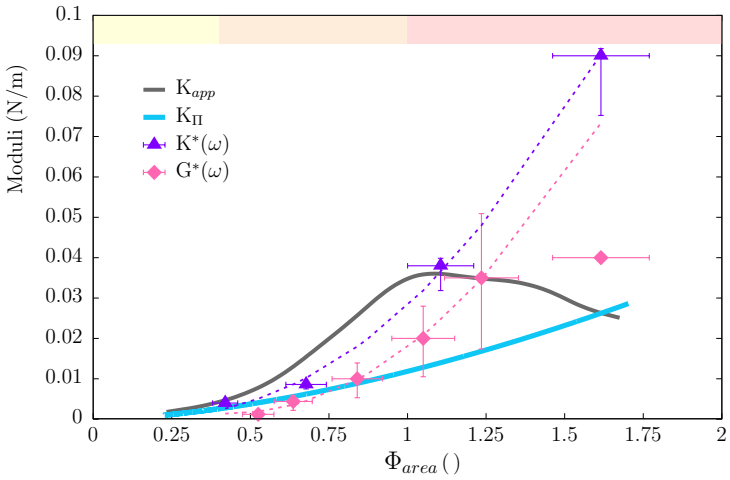

Figure 12: Summary of measured moduli as a function of surface coverage ϕ_{area} for the whole asphaltenes at the water-hexadecane interface. The intrinsic dilatational (K_i^*) and shear (G_i^*) moduli are both monotonically increasing functions of surface area fractions. The thermodynamic compressibility, 'Gibbs elasticity' (K_Π), accounts for a decreasing fraction of the elastic modulus. The apparent moduli K_{app} obtained by compression in a Langmuir through show a non-monotonic behaviour, due to the occurrence of complex deformations and buckling. The y-error bars represent the frequency-dependency of the moduli values, while the x-errorbars account for a $\pm$ 2Å^2 in the estimation of nano-aggregate monolayer coverage. The shaded-colored bar on the top of the plot reflects the same regions in Fig. 5.

These results shed a light on ill understood trend reported in literature regarding the relation between emulsion stability and interfacial rheology, namely that there is a maximum in apparent elastic dilatational modulus as a function of asphaltene (bulk) concentration [24], although emulsion stability continues to increase with asphaltene contents. In fact, the same trend is observed for the apparent compressional modulus K_{app} here (grey curve in Fig. 12): there is a maximum in K_{app}, corresponding to a minimum in compressibility, close to assumed monolayer coverage, but from our results we see that the dilatational modulus $K^*(\omega)$ increases further up to the highest coverages measured, while K_{app} continues to decrease. The way the apparent compressional modulus is typically measured in pendant drop or oscillating-barrier Langmuir trough most likely represents a combined response stemming from different contributions: the compressibility of the interface and possibly linear viscoelastic contributions from shear and compression as well. In the radial trough the kinematics are

clean and the deformation is purely isotropic, although the static and extra isotropic contributions are still coupled. From our rheology data we observe that the dilatational modulus $K^*(\omega)$ and the shear modulus $G^*(\omega)$ are monotonously increasing functions of coverage, as expected for a "hard" colloidal system. It can hence be expected that the deviatoric (purely rheological) surface stresses which appear as a boundary condition for the fluid flow in thin films during film drainage and coalescence will show a similar dependency on surface coverage, which correlates well with the reported increasing emulsion stability with increasing coverage. When measured with clean kinematics, the interfacial rheological properties increase monotonically and the reported non-monotonic evolutions of the apparent moduli are attributed to intricacies of the measurement techniques such as pendant drop or rectangular Langmuir throughs which have complex kinematics (mixed deformation fields and out of plane deformations) which obfuscates a clear assessment of mechanical effects[41,42].

Asphaltene subfractions

To investigate to what extent chemical heterogeneities leads to changes in the interfacial rheological behavior, different fractions as produced by the protocol in Fig. 1 and defined in Table 1 were used. Comparing the behaviour of these fractions should clarify if the interfacial response is mainly controlled by packing (SGR) or by interactions (gel). If the behaviour of the different fractions is similar, the interfacial crowding is the main mechanism. When significant effects of polarity are observed, it is likely that a physical network is responsible for gel formation. As can be seen from the elemental analysis in Table S1, all subfractions have in general a similar composition, yet they show a few noticeable variations. The irreversibly adsorbed subfraction has the highest H/C ratio, indicating a more aliphatic nature, and also significantly higher oxygen content, while the nickel and vanadium contents are the smallest among the subfractions. Conversely, the adsorbed subfraction is the richest in Ni and V, and has the highest heteroatom (S and N) contents. The bulk subfraction has lowest H/C ratio, indicating a higher amount of aromatic structures, as well as the lowest amount

of heteroatoms. From these results, it can also be inferred that the irreversibly adsorbed subfraction is the most polar one, followed by the adsorbed subfraction. The hydrodynamic radius (R_H) measured in a 0.1 wt% solution in toluene showed a broad size distribution for all subfractions over a range of $\sim$2 - 60Å^2, suggesting that samples contain both nanoaggregates as well as individual molecules[62]. Moreover, both adsorbed and irreversibly adsorbed fractions display higher average R_H than the bulk and whole asphaltenes, indicating that these two subfractions are more prone to form larger nanoaggregates, as has been previously shown for less aromatic asphaltenes[93].

Compression-expansion experiments

Compression experiments for the different subfractions were performed at the oil-water interfaces and the results are shown in Fig. 13. Tests were carried out starting from the same surface coverage in terms of mean molecular area (MMA of 91 ± 2 Å^2) for all subfractions, with initial surface pressures smaller than 1.0 mN/m for all curves. The inset shows a zoom in the region of 60 - 90 Å^2 where surface tension effects are still dominant.

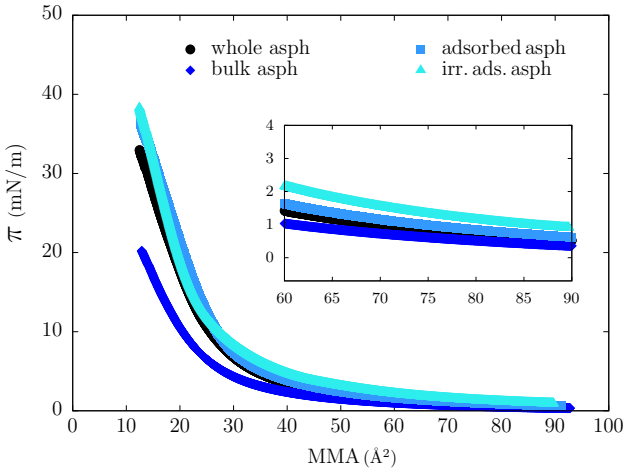

Figure 13: Compression experiments in Langmuir trough for comparison of the behavior of different subfractions at the oil-water interface. Inset shows a zoom in the region of 60-90Å^2 to highlight differences between the curves.

At a first glance, the four curves have the same overall shape showing no clear phase

transitions or collapse, indicating that despite the differences in chemical nature no fundamental changes in behavior are seen. It can be observed that the interfacial behaviour of the whole asphaltene seems to be dominated by the adsorbed and irreversibly adsorbed subfractions, while the bulk subfraction displays somewhat lower surface pressures and seems to be the least "interfacially active" subfraction, which is not unexpected when considering the fractionation process (Fig. 1). "Interfacial activity" in terms of the capacity of lowering of the interfacial energy per unit area can be better compared at lower coverages, shown in the inset of Fig. 13. In this range $> 60\,\text{Å}^2$ the interfacial tension at a given surface concentration differs less than $\pm\,2$mN/m. Moreover, the small values of Π suggest that nanoaggregates from fractionated asphaltenes are also not very efficient surfactants.

The difference between the magnitude of Π at the highest compression is striking: the maximum surface pressure value for the bulk subfraction is almost half of the other two subfractions. This is likely due to the more polar nature of the adsorbed and irreversibly adsorbed asphaltenes, where both subfractions experience more attractive interactions leading to enhanced mechanical stresses. Multiple cycle experiments were also performed for the different subfractions spread at the same mean molecular area (Figs. S10) and the results show similar tendencies as observed in Fig. 4b, namely reversibility of the compression for all cases and very small hysteresis.

It is worth noting that in experiments started at the same mass coverage (Fig. S11) the initial surface pressures are different and ranging from $0.9 \sim 4.0$ mN/m, and pronounced differences between the subfractions could be inferred from this plot. However, this is likely because starting at the same initial mass coverage for components having different molecular weight means that we start from different mean molecular area, and hence different packing states. As we have seen from the first part, it can be concluded that interfacial behavior of insoluble asphaltene layers is mainly governed by effects of dense packing.

Interfacial rheology

Interfacial rheology experiments were carried out at the same (estimated) area surface coverage to enable a direct comparison between subfractions. Dilatational and shear rheological properties of the different subfractions will be compared at coverages $11.8 \pm 0.5\,\text{Å}^2$. Dilatational frequency sweeps for the different subfractions are presented in Fig. 14. Here the measured dynamic moduli are compared to the apparent modulus obtained from a continuous compression K_{app} (dashed lines). Similar qualitative responses are observed for the subfractions, with the elastic dilatational modulus $K^{'}(\omega)$ being approximately constant and $K^{''}(\omega)$ increasing with frequency. It is clear that the dilatational behavior is dominated by rheology ($K^{'}(\omega) > K_{app}$), except for the bulk subfraction that exhibits fairly low moduli, indicating little resistance to being expanded. This might be due to the fact that this subfraction is the first one to be obtained upon fractionation and does not show any chemical features that would lead to interactions between nanoaggregates.

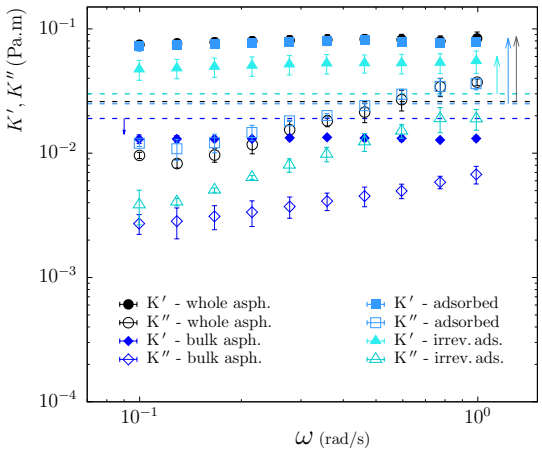

Figure 14: Interfacial dilatational frequency sweeps of the different subfractions at a coverage of $11.8 \pm 0.5\,\text{Å}^2$. The dashed lines represent the value of the apparent modulus K_{app} for each subfraction at this coverage.

Insoluble layers of the asphaltene subfractions were also studied in simple shear flow. Figure 15 presents results for oscillatory (a) frequency sweeps and (b) strain amplitude sweeps. Again a similar qualitative behavior is observed between all subfractions: in Fig. 15a,

$G_i' > G_i''$ throughout and the moduli display similar frequency dependency, and in Fig. 15b limiting strains of the linear viscoelastic regime are around 1%. In general, the values of the moduli from different subfractions vary within one order of magnitude for a given frequency and amplitude.

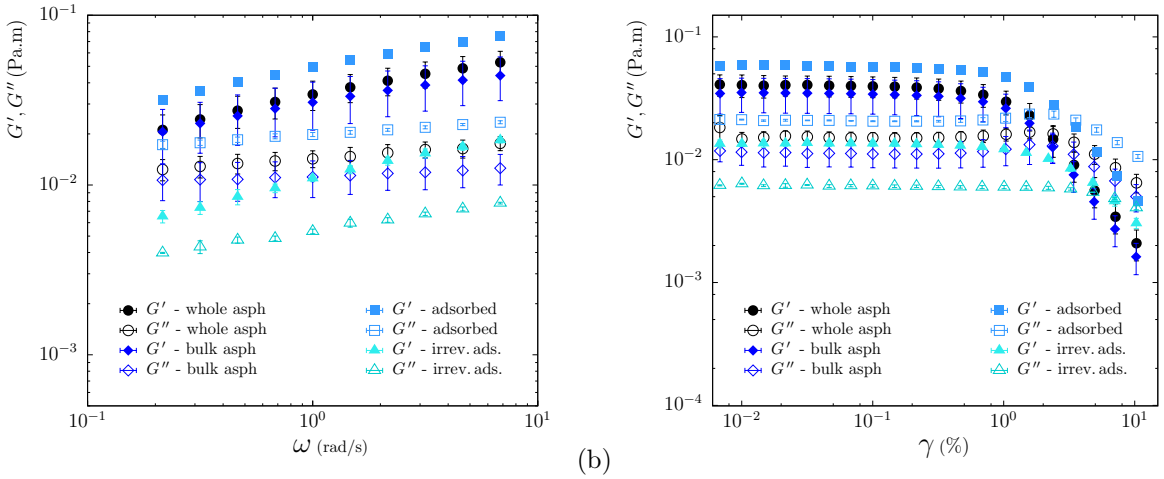

Figure 15: Interfacial shear rheology results of the different subfractions: (a) frequency sweeps ($\gamma_a = 0.02\%$) and (b) strain amplitude sweeps ($\omega = 2$ rad/s).

There are some minor differences. It is seen that the whole asphaltenes and the bulk subfraction display very similar results, while the adsorbed and irreversibly adsorbed present respectively the highest and the smallest moduli. Furthermore, the strain amplitude sweeps show a slight increase of G_i'' close to limiting strain amplitudes, with the adsorbed subfraction showing the most pronounced 'bump'. As previously discussed for the whole asphaltenes, this feature is most commonly seen in aggregated systems and it is consistent with the previous comments that this specific subfractions seems to exhibit more attractive interactions. The differences observed could also be attributed to the uncertainty in molecular weight values, that would in turn affect the actual area coverages.

Concluding, the general interfacial behavior at oil-water interfaces of the different subfractions is quite similar, notwithstanding some minor differences. In general, all subfractions show a similar viscoelastic behavior, in contrast to reports of quartz-crystal microbalance (QCM) experiments of asphaltenes adsorbed in solid steel surfaces[53], where from changes

in dissipation it was argued that the irreversibly adsorbed subfraction layer is viscoelastic, while the other subfractions form rather rigid layers. The data presented here are consistent with the conceptual Yen-Mullins model of aggregated asphaltenes, suggesting that chemical heterogeneities are not expected to play a big role. For crude oils with high asphaltene contents, molecules will likely aggregate in bulk and adsorb as nanoaggregates or clusters, which will lead to pronounced mechanical properties. On the contrary, if they adsorb as individual molecules, then a different type of stabilization takes place, with charges and functional groups possibly playing a bigger role. Indeed, it was recently reported[70] that no crumpling was observed at concentrations < 100ppm (when asphaltenes are likely present as single molecules), but show buckling and hence pronounced mechanical properties at higher concentrations.

Conceptually, dense insoluble asphaltene nanoaggregate interfaces resemble particle-laden interfaces under the conditions studied, and as a consequence it might be more relevant to treat asphaltene-stabilized emulsions akin to Pickering emulsions as opposed to being Marangoni-stabilized[94]. Unlike simple surfactant systems, where stabilization comes from the fact that interfaces are mobile and hence surfactants can move around and resist draining flows by Marangoni forces that oppose surface tension gradients, stress carrying interfaces will resist drainage flows due to the mechanically strong nature of the interfaces, as evidenced by the high shear and dilatational moduli. There are several arguments in favour of this picture, including i) relatively low surface activity of asphaltenes in terms of interfacial tension lowering vs. pronounced importance of mechanical properties (see Fig.12); ii) unlike surfactants, asphaltenes do not have a well-defined amphiphilic character[95]; iii) irreversible adsorption[21], which is a characteristic feature of particle-laden interfaces due to the high trapping energy ($\sim$ several k_BT); iv) comparison to model asphaltene compounds[96] - despite being very similar in the chemical nature, most likely these are usually present as individual monomers and thus do not adsorb as aggregates, which might explain the qualitative differences in interfacial behavior between model and indigenous asphaltenes; v) using

different subfractions to explore chemical heterogeneity did not yield significantly different results; vi) arrested coalescence as observed by Pauchard and coworkers[26,28].

Concluding remarks

In this work, we have presented an overview of the interfacial properties of model, Langmuir asphaltene layers at both water-air and water-oil interfaces. By controlling surface coverage and excluding effects of adsorption from bulk phases, interfaces populated by asphaltene nanoaggregates have been characterized using experiments with uniform kinematics, both in shear and dilation. The changes of the state variables, interfacial or surface tension, have been separated from the mechanical contributions to the surface stress. For oil-water interfaces the dilatational and shear moduli are monotonically increasing functions of surface coverage. Initially, asphaltenes behave as simple surfactants, however only decreasing slightly the surface energy of the interface and without showing any viscoelastic relaxation. The intrinsic surface activity is not very high. As the coverage is increased, the interface develops solid-like characteristics and starts to resist deformation, as evidenced by the rheological quantities. Below monolayer coverage, we observe a broad distribution of relaxation times as verified by the stretched decay and the agreement with a soft glassy model fit, which is in accordance with a picture of dense packing being the main cause of the response rather than the formation of a physical gel. Beyond assumed monolayer coverage, this behavior shifts to a more pronounced viscoelastic response and even higher moduli, likely due to the formation of multilayers, revealing a stronger interface that resists deformation until yielding. Yet insoluble asphaltenes layers are clearly rheologically very active.

Comparing the rheological properties of different subfractions, the properties of Langmuir asphaltene monolayers are shown to be governed by their surface coverage, and the packing of nanoaggregates is most likely the most important aspect. For spread layers also no time effects are observed, consistent with the surface coverage being the control parameter, so

in-plane crosslinking is an unlikely cause of the ageing observed in earlier literature. Of course, real crude oil possesses higher complexity and other effects such as of solubility of asphaltenes depending on crude oil composition (aliphatic/aromatic ratio), interplay with resins[97–99], the possible enhancement of emulsion stability due to the presence of fine inorganic solid particles[4,100], among others are still not clear. Albeit working with planar and model, insoluble interfaces that emphasize the colloidal nature of these asphaltene layers, these show significant solid-like behaviour with monotonic increases of moduli with surface concentration, which can be expected to remain the key parameter in determining the nature of the stress boundary condition governing the drainage of liquid during droplet-droplet interactions when asphaltenes are in a more complex environment.

Acknowledgement

The authors thank the JIP Electrocoalescence Consortium, "New Strategy for Separation of Complex Water-in-Crude Oil Emulsions: From Bench to Large Scale Separation" (NFR PETROMAKS) funded by Norwegian Research Council (Grant No. 255174) and the following industrial partners: Anvendt Teknologi AS, Equinor, NalcoChampion, Nouryon, and Sulzer. Discussions with Erik Björklund from Sulzer were much appreciated. We also gratefully acknowledge Stephan Busato for helping with the design and for making the elastic bands for radial trough experiments at the liquid-liquid interfaces.

Supporting Information Available

- Supporting Info

This material is available free of charge via the Internet at `http://pubs.acs.org/`.

References

(1) Sjöblom, J.; Aske, N.; Auflem, I.; Brandal, O.; Havre, T.; Saether, O.; Westvik, A.; Johnsen, E.; Kallevik, H. Our current understanding of water-in-crude oil emulsions. Recent characterization techniques and high pressure performance. *Advances in Colloid and Interface Science* **2003**, *100*, 399–473.

(2) Kokal, S. L. Crude Oil Emulsions: A State-of-the-Art Review. *SPE Production & Facilities* **2005**, *20*, 5–13.

(3) Strassner, J. E. Effect of pH on Interfacial Films and Stability of Crude Oil-Water Emulsions. *Journal of Petroleum Technology* **1968**, *20*, 303–312.

(4) Kilpatrick, P. K. Water-in-Crude Oil Emulsion Stabilization: Review and Unanswered Questions. *Energy & Fuels* **2012**, *26*, 4017–4026.

(5) Mullins, O. C. The Asphaltenes. *Annual Review of Analytical Chemistry* **2011**, *4*, 393–418.

(6) Langevin, D.; Argillier, J.-F. Interfacial behavior of asphaltenes. *Advances in Colloid and Interface Science* **2016**, *233*, 83–93.

(7) Schuler, B.; Meyer, G.; Peña, D.; Mullins, O. C.; Gross, L. Unraveling the Molecular Structures of Asphaltenes by Atomic Force Microscopy. *Journal of the American Chemical Society* **2015**, *137*, 9870–9876.

(8) Chacón-Patiño, M. L.; Rowland, S. M.; Rodgers, R. P. Advances in Asphaltene Petroleomics. Part 3. Dominance of Island or Archipelago Structural Motif Is Sample Dependent. *Energy & Fuels* **2018**, *32*, 9106–9120.

(9) Hoepfner, M. P.; Fávero, C. V. B.; Haji-Akbari, N.; Fogler, H. S. The Fractal Aggregation of Asphaltenes. *Langmuir* **2013**, *29*, 8799–8808.

(10) Rashid, Z.; Wilfred, C. D.; Gnanasundaram, N.; Arunagiri, A.; Murugesan, T. A comprehensive review on the recent advances on the petroleum asphaltene aggregation. *Journal of Petroleum Science and Engineering* **2019**, *176*, 249–268.

(11) Mullins, O. C. The Modified Yen Model. *Energy & Fuels* **2010**, *24*, 2179–2207.

(12) Gray, M. R.; Tykwinski, R. R.; Stryker, J. M.; Tan, X. Supramolecular Assembly Model for Aggregation of Petroleum Asphaltenes. *Energy & Fuels* **2011**, *25*, 3125–3134.

(13) Zhang, S.-F.; Sun, L.; Xu, J.; Wu, H.; Wen, H. Aggregate Structure in Heavy Crude Oil: Using a Dissipative Particle Dynamics Based Mesoscale Platform. *Energy & Fuels* **2010**, *24*, 4312–4326.

(14) Skartlien, R.; Simon, S.; Sjöblom, J. A DPD study of asphaltene aggregation: The role of inhibitor and asphaltene structure in diffusion-limited aggregation. *Journal of Dispersion Science and Technology* **2017**, *38*, 440–450.

(15) Silva, H. S.; Alfarra, A.; Vallverdu, G.; Bégué, D.; Bouyssiere, B.; Baraille, I. Asphaltene aggregation studied by molecular dynamics simulations: role of the molecular architecture and solvents on the supramolecular or colloidal behavior. *Petroleum Science* **2019**, *16*, 669–684.

(16) Ervik, A.; Lysgaard, M. O.; Herdes, C.; Jimenez-Serratos, G.; Müller, E. A.; Munkenjord, S. T.; Müller, B. A multiscale method for simulating fluid interfaces covered with large molecules such as asphaltenes. *Journal of Computational Physics* **2016**, *327*, 576–611.

(17) Chen, J.; Chen, J.; Zong, C.; Chen, S.; Chen, B.; Fang, S.; Xiang, W. Mesoscopic probes in asphaltenes nanoaggregate structure: from perpendicular to parallel orientation at the water-oil emulsions interface. *RSC Advances* **2017**, 38193–38203.

(18) Pieranski, P. Two-Dimensional Interfacial Colloidal Crystals. *Physical Review Letters* **1980**, *45*, 569–572.

(19) Yeung, A.; Dabros, T.; Czarnecki, J.; Masliyah, J. On the interfacial properties of micrometre-sized water droplets in crude oil. *Proceedings: Mathematical, Physical and Engineering Sciences* **1999**, *455*, 3709–3723.

(20) Jeribi, M.; Almir-Assad, B.; Langevin, D.; Hénaut, I.; Argillier, J.-F. Adsorption Kinetics of Asphaltenes at Liquid Interfaces. *Journal of Colloid and Interface Science* **2002**, *256*, 268–272.

(21) Freer, E. M.; Radke, C. J. Relaxation of asphaltenes at the toluene/water interface: diffusion exchange and surface rearrangement. *The Journal of Adhesion* **2004**, *80*, 481–496.

(22) McLean, J. D.; Kilpatrick, P. K. Effects of Asphaltene Solvency on Stability of Water-in-Crude-Oil Emulsions. *Journal of Colloid and Interface Science* **1997**, *189*, 242–253.

(23) Bouriat, P.; Kerri, N. E.; Graciaa, A.; Lachaise, J. Properties of a Two-Dimensional Asphaltene Network at the Water-Cyclohexane Interface Deduced from Dynamic Tensiometry. *Langmuir* **2004**, *20*, 7459–7464.

(24) Yarranton, H. W.; Sztukowski, D. M.; Urrutia, P. Effect of interfacial rheology on model emulsion coalescence I. Interfacial rheology. *Journal of Colloid and Interface Science* **2007**, *310*, 246–252.

(25) Verruto, V. J.; Kilpatrick, P. K. Water-in-Model Oil Emulsions Studied by Small-Angle Neutron Scattering: Interfacial Film Thickness and Composition. *Langmuir* **2008**, *24*, 12807–12822.

(26) Pauchard, V.; Rane, J. P.; Banerjee, S. Asphaltene-Laden Interfaces Form Soft Glassy

Layers in Contraction Experiments: A Mechanism for Coalescence Blocking. *Langmuir* **2014**, *30*, 12795–12803.

(27) Samaniuk, J. R.; Hermans, E.; Verwijlen, T.; Pauchard, V.; Vermant, J. Soft-glassy Rheology of Asphaltenes at Liquid Interfaces. *Journal of Dispersion Science and Technology* **2015**, *36*, 1444–1451.

(28) Pauchard, V.; Roy, T. Blockage of coalescence of water droplets in asphaltenes solutions: A jamming perspective. *Colloids and Surfaces A: Physicochemical and Engineering Aspects* **2014**, *443*, 410 – 417.

(29) Rocha, J. A.; Baydak, E. N.; Yarranton, H. W. What Fraction of the Asphaltenes Stabilizes Water-in-Bitumen Emulsions? *Energy & Fuels* **2018**, *32*, 1440–1450.

(30) Bouriat, P. Comment on "Mixture Effect on the Dilatation Rheology of Asphaltene-Laden Interfaces". *Langmuir* **2019**, *35*, 2451–2453.

(31) Chebel, N. A.; Piedfert, A.; Lalanne, B.; Dalmazzone, C.; Noik, C.; Masbernat, O.; Risso, F. Interfacial Dynamics and Rheology of a Crude-Oil Droplet Oscillating in Water at a High Frequency. *Langmuir* **2019**, *35*, 9441–9455.

(32) Simon, S.; Ruwoldt, J.; Sjöblom, J. A critical update of experimental techniques of bulk and interfacial components for fluid characterization with relevance to well fluid processing and transport. *Advances in Colloid and Interface Science* **2020**, *277*, 102120.

(33) Erni, P. Deformation modes of complex fluid interfaces. *Soft Matter* **2011**, *7*, 7586–7600.

(34) Fuller, G. G.; Vermant, J. Complex Fluid-Fluid Interfaces: Rheology and Structure. *Annual Review of Chemical and Biomolecular Engineering* **2012**, *3*, 519–543.

(35) Jaensson, N.; Vermant, J. Tensiometry and rheology of complex interfaces. *Current Opinion in Colloid and Interface Science* **2018**, *37*, 136–150.

(36) Spiecker, P. M.; Kilpatrick, P. K. Interfacial Rheology of Petroleum Asphaltenes at the Oil-Water Interface. *Langmuir* **2004**, *20*, 4022–4032.

(37) Fan, Y.; Simon, S.; Sjöblom, J. Interfacial shear rheology of asphaltenes at oil-water interface and its relation to emulsion stability: Influence of concentration, solvent aromaticity and nonionic surfactant. *Colloids and Surfaces A: Physicochemical and Engineering Aspects* **2010**, *366*, 120–128.

(38) Harbottle, D.; Chen, Q.; Moorthy, K.; Wang, L.; Xu, S.; Liu, Q.; Sjöblom, J.; Xu, Z. Problematic Stabilizing Films in Petroleum Emulsions: Shear Rheological Response of Viscoelastic Asphaltene Films and the Effect on Drop Coalescence. *Langmuir* **2014**, *30*, 6730–6738.

(39) Dicharry, C.; Arla, D.; Sinquin, A.; Graciaa, A.; Bouriat, P. Stability of water/crude oil emulsions based on interfacial dilatational rheology. *Journal of Colloid and Interface Science* **2006**, *297*, 785–791.

(40) Alvarez, G.; Poteau, S.; Argillier, J.-F.; Langevin, D.; Salager, J.-L. Heavy Oil-Water Interfacial Properties and Emulsion Stability: Influence of Dilution. *Energy & Fuels* **2009**, *23*, 294–299.

(41) Nagel, M.; Tervoort, T. A.; Vermant, J. From drop-shape analysis to stress-fitting elastometry. *Advances in Colloid and Interface Science* **2017**, *247*, 33–51.

(42) Knoche, S.; Vella, D.; Aumaitre, E.; Degen, P.; Rehage, H.; Cicuta, P.; Kierfeld, J. Elastometry of Deflated Capsules: Elastic Moduli from Shape and Wrinkle Analysis. *Langmuir* **2013**, *29*, 12463–12471.

(43) Kotula, A. P.; Anna, S. L. Insoluble layer deposition and dilatational rheology at a microscale spherical cap interface. *Soft Matter* **2016**, *12*, 7038–7055.

(44) Rodríguez-Hakim, M.; Anand, S.; Tajuelo, J.; Yao, Z.; Kannan, A.; Fuller, G. G. Asphaltene-induced spontaneous emulsification: Effects of interfacial co-adsorption and viscoelasticity. *Journal of Rheology* **2020**, *64*, 799–816.

(45) Verwijlen, T.; Imperiali, L.; Vermant, J. Separating viscoelastic and compressibility contributions in pressure-area isotherm measurements. *Advances in Colloid and Interface Science* **2014**, *206*, 428–436.

(46) Pepicelli, M.; Verwijlen, T.; Tervoort, T.; Vermant, J. Characterization and modelling of Langmuir interfaces with finite elasticity. *Soft Matter* **2017**, *13*, 5977–5990.

(47) Cicuta, P.; Terentjev, E. Viscoelasticity of a protein monolayer from anisotropic surface pressure measurements. *The European Physical Journal E* **2005**, *16*, 147–158.

(48) Vora, S.; Bognet, B.; Patanwala, H.; Young, C.; Chang, S.-Y.; Daux, V.; Ma, A. Global strain field mapping of a particle-laden interface using digital image correlation. *Journal of Colloid and Interface Science* **2018**, *509*, 94–101.

(49) Verruto, V. J.; Le, R. K.; Kilpatrick, P. K. Adsorption and Molecular Rearrangement of Amphoteric Species at Oil–Water Interfaces. *The Journal of Physical Chemistry B* **2009**, *113*, 13788–13799.

(50) Ruwoldt, J.; Subramanian, S.; Simon, S.; Oschmann, H.; Sjöblom, J. Asphaltene fractionation based on adsorption onto calcium carbonate: Part 3. Effect of asphaltenes on wax crystallization. *Colloids and Surfaces A: Physicochemical and Engineering Aspects* **2018**, *554*, 129 – 141.

(51) Yang, F.; Tchoukov, P.; Pensini, E.; Dabros, T.; Czarnecki, J.; Masliyah, J.; Xu, Z. Asphaltene Subfractions Responsible for Stabilizing Water-in-Crude Oil Emulsions. Part 1: Interfacial Behaviors. *Energy & Fuels* **2014**, *28*, 6897–6904.

(52) Qiao, P.; Harbottle, D.; Tchoukov, P.; Masliyah, J.; Sjöblom, J.; Liu, Q.; Xu, Z. Fractionation of Asphaltenes in Understanding Their Role in Petroleum Emulsion Stability and Fouling. *Energy & Fuels* **2017**, *31*, 3330–3337.

(53) Subramanian, S.; Simon, S.; Gao, B.; Sjöblom, J. Asphaltene fractionation based on adsorption onto calcium carbonate: Part 1. Characterization of sub-fractions and QCM-D measurements. *Colloids Surfaces A: Physicochem. Eng. Aspects* **2016**, *495*, 136–148.

(54) Pinto, F. E.; Barros, E. V.; Tose, L. V.; Souza, L. M.; Terra, L. A.; Poppi, R. J.; Vaz, B. G.; Vasconcelos, G.; Subramanian, S.; Simon, S.; Sjöblom, J.; Romão, W. Fractionation of asphaltenes in n-hexane and on adsorption onto CaCO3 and characterization by ESI(+)FT-ICR MS: Part I. *Fuel* **2017**, *210*, 790 – 802.

(55) Petkov, J. T.; Gurkov, T. D.; Campbell, B. E.; Borwankar, R. P. Dilatational and Shear Elasticity of Gel-Like Protein Layers on Air/Water Interface. *Langmuir* **2000**, *16*, 3703–3711.

(56) Gawrys, K. L.; Blankenship, G. A.; Kilpatrick, P. K. Solvent Entrainment in and Flocculation of Asphaltenic Aggregates Probed by Small-Angle Neutron Scattering. *Langmuir* **2006**, *22*, 4487–4497.

(57) Orbulescu, J.; Mullins, O. C.; Leblanc, R. M. Surface Chemistry and Spectroscopy of UG8 Asphaltene Langmuir Film, Part 1. *Langmuir* **2010**, *26*, 15257–15264.

(58) Fajardo-Rojas, F.; Pradilla, D.; Alvarez Solano, O. A.; Samaniuk, J. Probing Interfacial Structure and Dynamics of Model and Natural Asphaltenes at Fluid–Fluid Interfaces. *Langmuir* **2020**, *36*, 7965–7979.

(59) Pepicelli, M.; Jaensson, N.; Tregouët, C.; Schroyen, B.; Alicke, A.; Tervoort, T.; Monteux, C.; Vermant, J. Surface viscoelasticity in model polymer multilayers: From planar interfaces to rising bubbles. *Journal of Rheology* **2019**, *63*, 815–828.

(60) Vandebril, S.; Franck, A.; Fuller, G. G.; Moldenaers, P.; Vermant, J. A double wall-ring geometry for interfacial shear rheometry. *Rheologica Acta* **2010**, *49*, 131–144.

(61) Renggli, D.; Alicke, A.; Ewoldt, R.; Vermant, J. Operating windows for oscillatory interfacial shear rheology. *Journal of Rheology* **2020**, *64*, 141–160.

(62) Subramanian, S.; Sørland, G. H.; Simon, S.; Xu, Z.; Sjöblom, J. Asphaltene fractionation based on adsorption onto calcium carbonate: Part 2. Self-association and aggregation properties. *Colloids and Surfaces A: Physicochemical and Engineering Aspects* **2017**, *514*, 79 – 90.

(63) Chang, C.-C.; Nowbahar, A.; Mansard, V.; Williams, I.; Mecca, J.; Schmitt, A. K.; Kalantar, T. H.; Kuo, T.-C.; Squires, T. M. Interfacial Rheology and Heterogeneity of Aging Asphaltene Layers at the Water-Oil Interface. *Langmuir* **2018**, *34*, 5409–5415.

(64) Halperin, K.; Ketterson, J. B.; Dutta, P. A Study on the Mechanical Behavior of Surface Monolayers Using Orthogonal Wilhelmy Plates. *Langmuir* **1988**, *5*, 161–164.

(65) Zang, D. Y.; Rio, E.; Langevin, D.; Wei, B.; Binks, B. P. Viscoelastic properties of silica nanoparticle monolayers at the air-water interface. *The European Physical Journal E* **2010**, *31*, 125–134.

(66) Hua, Y.; Angle, C. W. Brewster Angle Microscopy of Langmuir Films of Athabasca Bitumens, n-C5 Asphaltenes, and SAGD Bitumen during Pressure-Area Hysteresis. *Langmuir* **2013**, *29*, 244–263.

(67) Orbulescu, J.; Mullins, O. C.; Leblanc, R. M. Surface Chemistry and Spectroscopy of UG8 Asphaltene Langmuir Film, Part 2. *Langmuir* **2010**, *26*, 15265–15271.

(68) Zhang, L. Y.; Xu, Z.; Masliyah, J. Langmuir and Langmuir-Blodgett Films of Mixed Asphaltene and Demulsifier. *Langmuir* **2003**, *19*, 9730–9741.

(69) Rane, J. P.; Harbottle, D.; Pauchard, V.; Couzis, A.; Banerjee, S. Adsorption Kinetics of Asphaltenes at the Oil-Water Interface and Nanoaggregation in the Bulk. *Langmuir* **2012**, *28*, 9986–9995.

(70) You, J.; Li, C.; Liu, D.; Yang, F.; Sun, G. Influence of the Aggregation State of Asphaltenes on Structural Properties of the Model Oil/Brine Interface. *Energy & Fuels* **2019**, *33*, 2994–3002.

(71) Yarranton, H. W.; Hussein, H.; Masliyah, J. H. Water-in-Hydrocarbon Emulsions Stabilized by Asphaltenes at Low Concentrations. *Journal of Colloid and Interface Science* **2000**, *228*, 52–63.

(72) Rocha, J. A.; Baydak, E. N.; Yarranton, H. W.; Sztukowski, D. M.; Ali-Marcano, V.; Gong, L.; Shi, C.; Zeng, H. Role of Aqueous Phase Chemistry, Interfacial Film Properties, and Surface Coverage in Stabilizing Water-in-Bitumen Emulsions. *Energy & Fuels* **2016**, *30*, 5240–5252.

(73) Rane, J. P.; Pauchard, V.; Couzis, A.; Banerjee, S. Interfacial Rheology of Asphaltenes at Oil-Water Interfaces and Interpretation of the Equation of State. *Langmuir* **2013**, *29*, 4750–4759.

(74) Lin, Y.-J.; Barman, S.; He, P.; Zhang, Z.; Cristopher, G. F.; Biswal, S. L. Combined interfacial shear rheology and microstructure visualization of asphaltenes at air-water and oil-water interfaces. *Journal of Rheology* **2018**, *62*, 1–10.

(75) Fainerman, V. B.; Vollhardt, D. Equations of State for Langmuir Monolayers with Two-Dimensional Phase Transitions. *J. Phys. Chem. B* **1999**, *103*, 145–150.

(76) Imperiali, L.; Liao, K.-H.; Clasen, C.; Fransaer, J.; Macosko, C. W.; Vermant, J. Interfacial Rheology and Structure of Tiled Graphene Oxide Sheets. *Langmuir* **2012**, *28*, 7990–8000.

(77) Van Hooghten, R.; Imperiali, L.; Boeckx, V.; Sharma, R.; Vermant, J. Rough nanoparticles at the oil–water interfaces: their structure, rheology and applications. *Soft Matter* **2013**, *9*, 10791–10798.

(78) Jestin, J.; Simon, S.; Zupancic, L.; Barré, L. A Small Angle Neutron Scattering Study of the Adsorbed Asphaltene Layer in Water-Hydrocarbon Emulsions: Structural Description Related to Stability. *Langmuir* **2007**, *23*, 10471–10478.

(79) Alvarez, G.; Jestin, J.; Argillier, J.; Langevin, D. Small-Angle Neutron Scattering Study of Crude Oil Emulsions: Structure of the Oil-Water Interfaces. *Langmuir* **2009**, *25*, 3985–3990.

(80) Sjöblom, J.; Simon, S.; Xu, Z. Model molecules mimicking asphaltenes. *Advances in Colloid and Interface Science* **2015**, *218*, 1–16.

(81) Zhang, S.; Zhang, L.; Lu, X.; Shi, C.; Tang, T.; Wang, X.; Huang, Q.; Zeng, H. Adsorption kinetics of asphaltenes at oil/water interface: Effects of concentration and temperature. *Fuel* **2018**, *212*, 387–394.

(82) Bochner, S.; Merola, M.; Vlassopoulos, D.; Fuller, G. G. Droplet Coalescence and Spontaneous Emulsification in the Presence of Asphaltene Adsorption. *Langmuir* **2017**, *33*, 10501–10510.

(83) Duboue, J.; Bourrel, M.; Carreras, E. S.; Klimenko, A.; Agenet, N.; Passade-Boupat, N.; Lequeux, F. Auto-Emulsification of Water at Crude Oil/Water Interface: a Mechanism Driven by Osmotic Gradient. *Energy & Fuels* **2019**, *33*, 7020–7027.

(84) Sollich, P.; Laqueux, F.; Hébraud, P.; Cates, M. Rheology of Soft Glassy Materials. *Physical Review Letters* **1997**, *78*, 2020–2023.

(85) Sollich, P. Rheological constitutive equation for a model of soft glassy materials. *Physical Review E* **1998**, *58*, 738–759.

(86) Fielding, S.; Sollich, P.; Cates, M. Aging and rheology in soft materials. *Journal of Rheology* **2000**, *44*, 323–369.

(87) Koumakis, N.; Petekidis, G. Two step yielding in attractive colloids: transition from gels to attractive glasses. *Soft Matter* **2011**, *7*, 2456–2470.

(88) Donley, G. J.; Singh, P. K.; Shetty, A.; Rogers, S. A. Elucidating the G" overshoot in soft materials with a yield transition via a time-resolved experimental strain decomposition. *Proceedings of the National Academy of Sciences* **2020**, *117*, 21945–21952.

(89) Thompson, R. L.; sica, L. U. R.; de Souza Mendes, P. R. The yield stress tensor. *Journal of Non-Newtonian Fluid Mechanics* **2018**, *261*, 211–219.

(90) de Cagny, H.; Fazilati, M.; Habibi, M.; Denn, M. M.; Bonn, D. The yield normal stress. *Journal of Rheology* **2019**, *63*, 285–290.

(91) Beltramo, P. J.; Gupta, M.; Alicke, A.; Liascukiene, I.; Gunes, D. Z.; Baroud, C. N.; Vermant, J. Arresting dissolution by interfacial rheology design. *Proceedings of the National Academy of Sciences* **2017**, *114*, 10373–10378.

(92) Tervoort, T. A.; Klompen, E. T. J.; Govaert, L. E. A multi-mode approach to finite, three-dimensional, nonlinear viscoelastic behavior of polymer glasses. *Journal of Rheology* **1996**, *40*, 779–797.

(93) Yarranton, H. W. et al. On the Size Distribution of Self-Associated Asphaltenes. *Energy & Fuels* **2013**, *27*, 5083–5106.

(94) Tambe, D. E.; Sharma, M. M. The effect of colloidal particles on fluid-fluid interfacial properties and emulsion stability. *Advances in Colloid and Interface Science* **1994**, *52*, 1–63.

(95) Czarnecki, J.; Tchoukov, P.; Dabros, T.; Xu, Z. Role of Asphaltenes in Stabilisation of

Water in Crude Oil Emulsions. *The Canadian Journal of Chemical Engineering* **2013**, *91*, 1365–1371.

(96) Pradilla, D.; Simon, S.; Sjöblom, J.; Samaniuk, J.; Skrzypiec, M.; Vermant, J. Sorption and Interfacial Rheology Study of Model Asphaltene Compounds. *Langmuir* **2016**, *32*, 2900–2911.

(97) Gafonova, O. V.; Yarranton, H. W. The Stabilization of Water-in-Hydrocarbon Emulsions by Asphaltenes and Resins. *Journal of Colloid and Interface Science* **2001**, *241*, 469–478.

(98) Spiecker, P.; Gawrys, K. L.; Trail, C. B.; Kilpatrick, P. K. Effects of petroleum resins on asphaltene aggregation and water-in-oil emulsion formation. *Colloids and Surfaces A: Physicochemical and Engineering Aspects* **2003**, *220*, 9 – 27.

(99) Liu, D.; Li, C.; Yang, F.; Sun, G.; You, J.; Cui, K. Synergetic effect of resins and asphaltenes on water/oil interfacial properties and emulsion stability. *Fuel* **2019**, *252*, 581–588.

(100) Menon, V. B.; Wasan, D. T. A Review of the Factors Affecting the Stability of Solid-Stabilized Emulsions. *Separation Science and Technology* **1988**, *23*, 2131–2142.

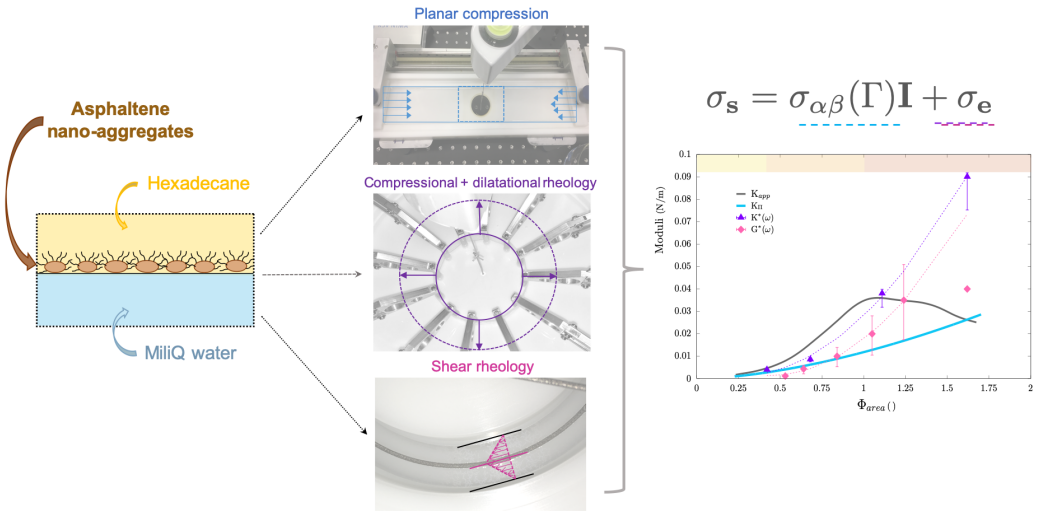

Figure 16: For Table of Contents Only